Technology

Developmental Cell

Programmable Extracellular Vesicles for Macromolecule Delivery and Genome Modifications

Graphical Abstract

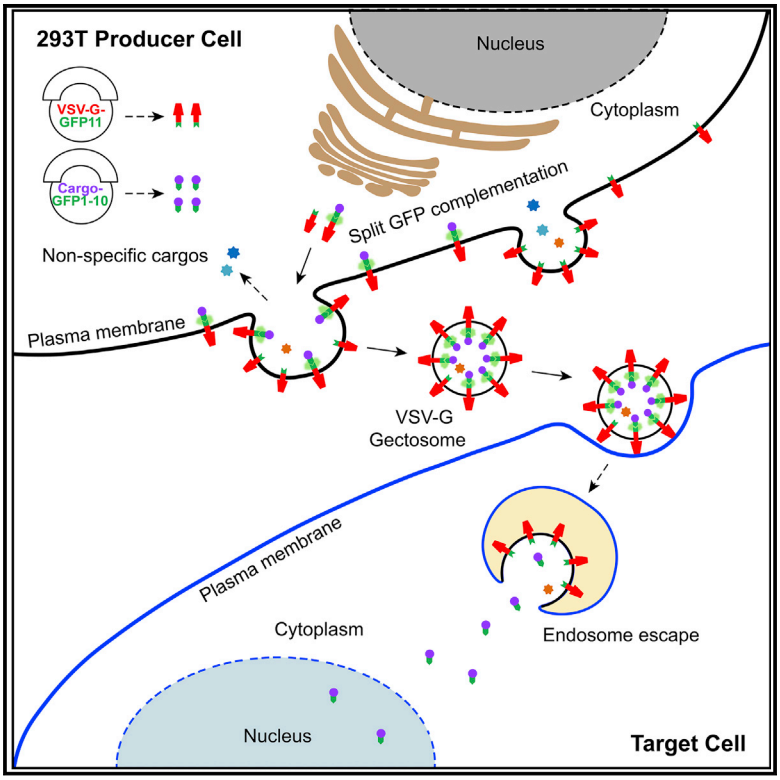

Highlights

- Gectosomes are EVs containing a specific cargo tethered to VSV-G via a split GFP
- Gectosomes can be purified, quantified, and modeled
- Gectosomes can deliver enzymes, RNAi, and Cas9 RNPs more efficiently than exosomes
- Active loading of Gectosomes reduces passive incorporation of cellular proteins

Authors

Xiaojuan Zhang, Quanbin Xu, Zhike Zi, ..., Lauren Crisman, Jingshi Shen, Xuedong Liu

Correspondence

xuedong.liu@colorado.edu

In Brief

Zhang et al. develop engineered extracellular vesicles (EVs), which allow efficient cargo loading and endosomal escape simultaneously for the intracellular delivery of macromolecules. They show that these programmable EVs improve the specificity of cargo loading and efficiency of delivering functional proteins or RNPs into cells and mice.

Zhang et al., 2020, Developmental Cell *55*, 1–18
December 21, 2020
https://doi.org/10.1016/j.devcel.2020.11.007

CellPress

Please cite this article in press as: Zhang et al., Programmable Extracellular Vesicles for Macromolecule Delivery and Genome Modifications, Developmental Cell (2020), https://doi.org/10.1016/j.devcel.2020.11.007

Developmental Cell

CellPress

Technology

Programmable Extracellular Vesicles for Macromolecule Delivery and Genome Modifications

Xiaojuan Zhang,[1,5] Quanbin Xu,[1,5] Zhike Zi,[2,3] Zeyu Liu,[1] Chun Wan,[4] Lauren Crisman,[4] Jingshi Shen,[4] and Xuedong Liu[1,6,*]

[1]Department of Biochemistry, University of Colorado, Boulder, CO 80303, USA
[2]Max Planck Institute for Molecular Genetics, Otto Warburg Laboratory, 14195 Berlin, Germany
[3]German Federal Institute for Risk Assessment, Department of Experimental Toxicology and ZEBET, 10589 Berlin, Germany
[4]Department of MCD-Biology, University of Colorado, Boulder, CO 80309, USA
[5]These authors contributed equally
[6]Lead Contact
*Correspondence: xuedong.liu@colorado.edu
https://doi.org/10.1016/j.devcel.2020.11.007

SUMMARY

Getting large macromolecules through the plasma membrane and endosomal barriers remains a major challenge. Here, we report a generalizable method of delivering proteins and ribonucleoproteins (RNPs) to cells *in vitro* and mouse liver tissue *in vivo* with engineered ectosomes. These ectosomes, referred to as "Gectosomes," are designed to co-encapsulate vesicular stomatitis virus G protein (VSV-G) with bioactive macromolecules via split GFP complementation. We found that this method enables active cargo loading, improves the specific activity of cargo delivery, and facilitates Gectosome purification. Experimental and mathematical modeling analyses suggest that active cargo loading reduces non-specific encapsulation of cellular proteins, particularly nucleic-acid-binding proteins. Using Gectosomes that encapsulate Cre, Ago2, and SaCas9, we demonstrate their ability to execute designed modifications of endogenous genes in cell lines *in vitro* and mouse liver tissue *in vivo*, paving the way toward applications of this technology for the treatment of a wide range of human diseases.

INTRODUCTION

The capability to deliver macromolecules such as proteins and nucleic acids into mammalian cells is of considerable interest to researchers and pharmaceutical industries. Innovative methods for gene modification and interfering with mRNA expression have become nearly indispensable tools for biomedical research (Doudna and Charpentier, 2014; Shalem et al., 2015). All these methods rely on the delivery of nucleic acids, proteins, or ribonucleoprotein (RNP) to the intracellular space of target cells, which is limited because the plasma and the endosome membrane are mostly impermeable to biologics. Finding ways to circumvent these barriers to deliver biomolecules in a pharmacologically consistent manner remains a significant challenge (Cocucci and Meldolesi, 2015; Fu et al., 2014; Maeder and Gersbach, 2016).

Extracellular vesicles (EVs) are heterogeneous, nano-sized membrane vesicles that are either constitutively or inducibly released by all cell types (Mathieu et al., 2019; Raposo and Stoorvogel, 2013; van Niel et al., 2018). Since EVs are increasingly being recognized as a native means of transporting bioactive molecules between cells, there is a growing interest in exploring EVs as delivery vehicles for therapeutics. However, several critical issues need to be addressed to realize EVs' translational potentials. First, various EVs, including exosomes, ectosomes/microvesicles, apoptotic bodies, and exomeres, are present in conditioned media or bodily fluids (Jeppesen et al., 2019; Mathieu et al., 2019). Methods to separate and purify each entity in sufficient quantities remain elusive (Tkach and Théry, 2016). Second, the specific activity of EVs tends to be low due to the heterogeneity of their cargos. In certain applications, loading exosomes with siRNA *in vitro* significantly improves the specific activity and efficacy of encapsulated therapeutic nucleic acid (Kamerkar et al., 2017). However, it is unclear whether this strategy can be extended to larger biomolecules such as proteins or RNP. Finally, proteomics and RNA-seq analyses reveal a great deal of diversity and heterogeneity of EV composition (Haraszti et al., 2016; Jeppesen et al., 2019; Kowal et al., 2016; Mangeot et al., 2004; Mathieu et al., 2019). Challenges remain to gain control of the molecular cargo encapsulated by each type of vesicle and to reduce the heterogeneity of EV composition.

Here, we report a general method for making programmable, highly fusogenic vesicles, which we call "Gectosomes" (VSV-G protein ectosomes), as vehicles for the dose-controlled delivery of bioactive macromolecules *in vitro* and *in vivo*. Borrowing from mechanisms of vesicular stomatitis viral delivery and proficient fusogenic activity of vesicular stomatitis virus G protein (VSV-G), we

Please cite this article in press as: Zhang et al., Programmable Extracellular Vesicles for Macromolecule Delivery and Genome Modifications, Developmental Cell (2020), https://doi.org/10.1016/j.devcel.2020.11.007

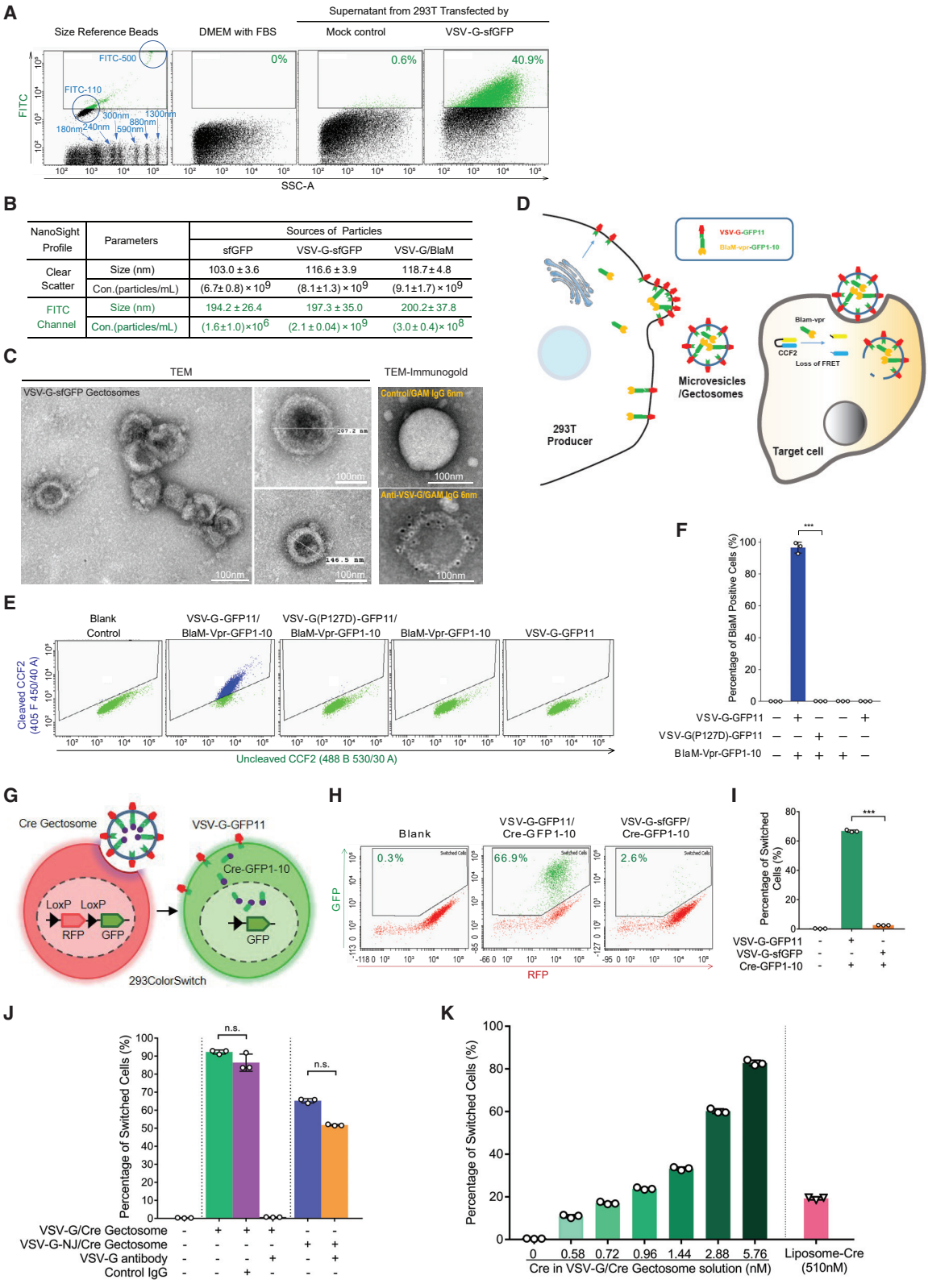

NanoSight Profile	Parameters	Sources of Particles		
		sfGFP	VSV-G-sfGFP	VSV-G/BlaM
Clear Scatter	Size (nm)	103.0 ± 3.6	116.6 ± 3.9	118.7 ± 4.8
	Con.(particles/mL)	$(6.7 \pm 0.8) \times 10^9$	$(8.1 \pm 1.3) \times 10^9$	$(9.1 \pm 1.7) \times 10^9$
FITC Channel	Size (nm)	194.2 ± 26.4	197.3 ± 35.0	200.2 ± 37.8
	Con.(particles/mL)	$(1.6 \pm 1.0) \times 10^6$	$(2.1 \pm 0.04) \times 10^9$	$(3.0 \pm 0.4) \times 10^8$

Figure 1. Development of a Two-Component Fluorescent Gectosome for Intercellular Transfer of Specific Proteins

(A) The size distribution of VSV-G-sfGFP particles by flow cytometry using FACSAria Fusion Cell Sorter. Size reference beads were used as the standard. Dot plots are representative of three individual experiments.

(legend continued on next page)

Please cite this article in press as: Zhang et al., Programmable Extracellular Vesicles for Macromolecule Delivery and Genome Modifications, Developmental Cell (2020), https://doi.org/10.1016/j.devcel.2020.11.007

developed an active cargo-loading strategy for Gectosomes using the split GFP system (Cabantous et al., 2005). Modeling and experimental studies show that active loading of Gectosomes via GFP complementation greatly increases the efficiency of cargo delivery to target cells and reduces non-specific encapsulation of cellular proteins. We demonstrated the versatility and broad applicability of this approach by the successful intracellular delivery of cytosolic and nuclear enzymes, resulting in the execution of DNA recombination, RNA interference, and gene editing in cultured cells and mice liver tissues *in vivo*. Since Gectosomes are genetically encoded, highly programmable, easy to prepare, and amenable to purification based on their cargo, this approach simplifies genome modification experiments and can be adapted to wide-ranging research and possible therapeutic applications.

Design

Delivering proteins and nucleic acids into the cytosol and nucleus is limited by the plasma and the endosome membrane barriers. EVs are capable of overcoming these barriers of entry to mediate intercellular transfer of the encapsulated macromolecular cargos. However, the major challenges for delivering intracellular biologics with EVs are the lack of control of the cargo content and the inability to isolate EVs loaded with defined cargo. We have developed an engineering method for making a specific type of EVs called Gectosomes, which facilitate cargo loading and their endosomal escape simultaneously. Gectosomes contain two major components: an engineered VSV-G and the cargo of interest tethered to one another via split GFP. Complementation of split GFP enables more efficient loading of the specific cargo and purification of desired fluorescent Gectosomes. We validated the functionality of engineered Gectosomes for delivering proteins or protein/RNA complexes designed to modify genotypes in mammalian cells *in vitro* and live animals *in vivo*.

RESULTS

Overexpression of VSV-G in Human Cells Elevates the Production of VSV-G-Containing EVs

Enveloped viruses often make use of their virus-encoded fusion protein to facilitate membrane fusion with host cells during infection (Albertini et al., 2012). VSV-G is one of the best-studied viral fusion proteins and is frequently used for pseudotyping retroviral or lentiviral particles to enable their entry into a broad range of cell types (Hirschberg et al., 1998; Lodish and Weiss, 1979). During our investigation of the pseudotyping activity of superfolder GFP tagged VSV-G (VSV-G-sfGFP), we noticed that copious amounts of small fluorescence particles ranging in size between 100 and 1,000 nm were present in the culture media from cells transfected solely with VSV-G-sfGFP by flow cytometry analysis (Figure 1A). To characterize these particles, we transiently transfected 293T cells with sfGFP or VSV-G-sfGFP expression vectors (Figure S1A) and harvested supernatants for NanoSight tracking analysis (NTA) (Figures 1B and S1B). We found that supernatant from VSV-G-sfGFP-transfected cells contained ~2 × 10^9 particles per mL with an average size of ~200 nm in the GFP fluorescence channel. In contrast, only ~1.6 × 10^6 particles per mL were detected in the same channel for the control transfection with sfGFP. The total number of EV particles per mL present in the media was comparable based on the particle counts in the clear channel (Figure 1B). Thus, VSV-G transfection favors the production of fluorescent vesicles by ~1,000-fold in 293T cells.

To determine whether VSV-G is present on the fluorescent vesicles, we incubated the VSV-G-sfGFP and the control supernatants with magnetic beads coated with a monoclonal antibody (8G5F11) against VSV-G (Lefrancois and Lyles, 1982). Strong bead fluorescence was observed with VSV-G-sfGFP supernatant but in neither the control nor beads without antibody, suggesting VSV-G is present on the surface of these particles (Figure S1C). To examine the morphology of these fluorescent vesicles, we performed transmission electron microscopy (TEM) and VSV-G immunogold labeling studies with the immunopurified vesicles (Figure 1C). The imaged particles show the expected round-shaped vesicles with an average diameter ~128 nm, which is slightly smaller than the average size determined by NTA or flow cytometry and could be due to the effects of sample fixation. Immunogold labeling with an anti-VSV-G antibody demonstrates that VSV-G is present on the surface of the vesicle (Figure 1C). These results show that VSV-G promotes the robust production of EVs enriched with this protein on the surface. Hereafter, we refer to VSV-G-containing EVs as "Gectosomes" for viral G-protein-containing ectosomes.

(B) Nanoparticle tracking analysis of the size distributions and concentrations of extracellular vesicles in the supernatants from sfGFP, VSV-G-sfGFP, or VSV-G-GFP11/BlaM-Vpr-GFP1-10-transfected cells. Data are mean ± SD for technical replicates (n = 3) and are representative of 10 individual experiments.
(C) Representative TEM and TEM immunogold images of VSV-G-sfGFP vesicles. Primary antibody: 8G5F11 VSV-G antibody; secondary antibody: goat anti-mouse IgG/M 6 nm.
(D) Schematic illustration showing VSV-G Gectosome-mediated BlaM protein transduction and detection in the target cell. The schematic model is not drawn to the scale.
(E and F) Flow cytometric analysis of CCF2-AM dye-loaded target HeLa cells (~3 × 10^5) incubated with vesicles collected from the supernatants of the same number of producer 293T cells (~10^6) transfected with the same amount of plasmids as shown. Representative dot plots and the quantification of BlaM-positive cells are reported (mean ± SD, n = 3). Data are representative of two individual experiments.
(G) Schematic diagram of the Cre transduction experiment (not to scale).
(H and I) Flow cytometric analysis of the color conversion of target cell 293ColorSwitch. 293ColorSwitch cells (~1 × 10^5) were treated for 48 h with extracellular vesicles (total particle number, ~4 × 10^9; GFP-positive particle number, ~4 × 10^8) collected from supernatants of 293T cells transfected with plasmids as shown. Data are mean ± SD (n = 3), and dot plots are representative of three individual experiments.
(J) Color conversion of target 293ColorSwitch cell (~1 × 10^5) with VSV-G/Cre Gectosomes (~8 × 10^8) or VSV-G-NJ/Cre Gectosomes (~8 × 10^8) in the presence of VSV-G antibody (8G5F11, 1:100) or control IgG; VSV-G-NJ is the G protein from vesicular stomatitis virus New Jersey strain. Data are mean ± SD (n = 3).
(K) Performance of Gectosomes versus artificial liposomes in Cre delivery to 293ColorSwitch cells. The plot shows the percentage of cells switched upon exposure to the indicated liposomes or Gectosomes containing the indicated amount of Cre as determined by flow cytometry analysis. Data are mean ± SD (n = 3). Statistical significance for (F), (I), and (J) was assessed using Student's t test, ***p < 0.001; n.s., not significant.
See also Figures S1 and S2.

Please cite this article in press as: Zhang et al., Programmable Extracellular Vesicles for Macromolecule Delivery and Genome Modifications, Developmental Cell (2020), https://doi.org/10.1016/j.devcel.2020.11.007

Development of Two-Component Fluorescent Gectosomes for Intercellular Transfer of Specific Proteins

Previous work showed that highly concentrated VSV-G EVs could mediate intercellular transfer of VSV-G and a variety of cellular proteins with low selectivity (Mangeot et al., 2011). Passive loading of VSV-G and cargos into vesicles makes these type of EVs highly heterogeneous and low efficiency for delivering specific cargo proteins. We aimed to develop an active loading strategy to recruit specific proteins into Gectosomes and enhance the specificity of cargo delivery. To this end, we used a split GFP system as the building block to construct a two-component Gectosome (Figure S1D, middle panel). Waldo and colleagues discovered that GFP could be split between the tenth and eleventh β-strands, resulting in separate constructs of a 16-amino acid (aa) fragment (GFP11) and the rest of the protein (GFP1-10) (Cabantous et al., 2005). Without the 16-aa peptide, GFP1-10 is nearly non-fluorescent. Upon co-expression of both fragments in cells, GFP11 binds GFP1-10 to reconstitute a functional, fluorescent GFP molecule. To determine whether the split GFP system could be used to bridge VSV-G and its binding partners in cells, we fused VSV-G with GFP11 at its C terminus (VSV-G-GFP11) and a β-lactamase-vpr reporter (BlaM-Vpr) with GFP1-10 at its C terminus (BlaM-Vpr-GFP1-10) (Figure 1D). 293T cells exhibited higher GFP fluorescence when VSV-G-GFP11 and BlaM-Vpr-GFP1-10 were transfected together compared with those that were transfected individually by flow cytometry (Figure S1A, green versus black traces) or confocal microscopy analyses (Figure S1E). These results confirm that VSV-G can find its intended cargo protein in cells.

To deliver encapsulated cargos to target cells, two-component Gectosomes need to be efficiently released from the producer 293T cells (Figure 1D). Supernatant from 293T cells transfected with the split GFP constructs was collected and subjected to NTA. As expected, VSV-G-GFP11/BlaM-Vpr-GFP1-10 particles (VSV-G/BlaM Gectosomes) are fluorescent, and their average size was similar to VSV-G-sfGFP particles (sfGFP Gectosomes), although the yield was slightly lower (3×10^8 particles/mL) (Figures 1B and S1B). To confirm the secretion and validate the biochemical composition of two-component Gectosomes, we performed subcellular fractionations followed by western blotting analysis. The result verified that VSV-G and BlaM are released from cells and present in the extracellular vesicle fractions (Figure S1F). To test whether two-component Gectosomes can transfer encapsulated cargo proteins from producer cells (293T) to target cells (HeLa), we incubated VSV-G/BlaM Gectosomes with HeLa cells. BlaM-Vpr reporter was selected because its enzyme activity can be easily measured by flow cytometry with CCF2-AM, a cell-permeable fluorescence resonance energy transfer (FRET) substrate, which consists of a cephalosporin core linking 7-hydroxycoumarin to fluorescein (Cavrois et al., 2002). BlaM catalyzes the reaction that severs the linkage between the two dyes leading to a loss of FRET so that exciting the coumarin at 409 nm now produces a blue fluorescence signal at 447 nm instead of the FITC signal at 488 nm. As shown in Figures 1E and 1F, only supernatant from 293T cells co-transfected with both constructs is capable of delivering BlaM to HeLa or 293T cells (Figures S1G and S1H). Moreover, cleavage of CCF2-AM is BlaM specific as Gectosomes produced by co-transfection with Cre-GFP1-10 (see below) have minimal activity (Figures S1G and S1H). As a control, we included a VSV-G mutant (P127D) shown to be defective in membrane fusion (Votteler et al., 2016). This mutant does not affect Gectosomes production or release from the producer cells (Figures 1E, S1A, S1E, and S1F). However, BlaM Gectosomes with fusion deficient VSV-G (P127D)-GFP11 fail to mediate the transfer of BlaM-Vpr-GFP1-10 to target cells (Figures 1E and 1F). These results suggest fusion is critical for Gectosomes cargo delivery, which is consistent with the role of VSV-G in mediating endosome escape of viral particles (Weissenhorn et al., 2007, 2013).

Robust and Dose-Controlled Intracellular Delivery of Macromolecules by Gectosomes

For exogenous proteins or nucleic acids to reach their intracellular targets, EVs need to fuse with the target cell either at the plasma membrane or inside the endosome following endocytosis. To further evaluate the capability of Gectosome delivery, we tested whether proteins that act on nuclear targets can be transferred from producer cells to target cells. Cre recombinase was selected for these studies since the function of Cre can be readily measured with 293ColorSwitch cells, which stably express a color switch reporter (Zomer et al., 2015). Upon Cre uptake, cells switch from a strong RFP to a GFP signal due to the excision of a floxed RFP-STOP cassette (Zomer et al., 2015) (Figure 1G). We fused Cre with GFP1-10 (Cre-GFP1-10) and co-expressed it with VSV-G-GFP11 in 293T cells (Figure S2A). As with VSV-G/BlaM Gectosomes, the fluorescent Cre Gectosomes were produced massively (~3.8×10^9 particles/mL). The average size of the Cre Gectosomes is about ~185 nm in diameter, but the particles appear to be more homogeneous (Figure S2B) by NTA analysis. To determine whether split GFP enables higher efficiency of Cre delivery, we incubated comparable numbers of Gectosomes from mock, VSV-G-GFP11/Cre-GFP1-10, and VSV-G-sfGFP/Cre-GFP1-10 with 293ColorSwitch cells for 48 h. We found that 66.9% of 293ColorSwitch cells were switched to GFP with Cre Gectosomes, while vesicles from untethered VSV-G-sfGFP/Cre-GFP1-10 resulted in only 2.6% switch, presumably due to passive cargo loading (Figures 1H and 1I). The effect of Cre-mediated recombination and the time course of this switching process were confirmed by confocal microscopy and flow cytometry respectively (Figures S2C–S2E). The same vesicles produced only background fluorescent signals in control 293T cells (Figure S2D). As a control, we also compared two-component Cre Gectosomes with one-component Gectosomes (i.e., direct VSV-G-Cre fusion, Figures S2F and S2G). No significant cell switch was observed with one-component VSV-G-Cre Gectosomes. These results indicate that bioactive Cre delivered by two-component Gectosomes efficiently enters the nucleus to mediate Cre-lox recombination in target cells and that active loading of Cre via split GFP greatly increases (~26-fold) the efficiency of this process.

Cellular uptake of Gectosomes may require specific interaction between VSV-G and receptor proteins present on the surface of target cells. The specificity and requirements of VSV-G for Gectosome delivery of Cre were investigated with a variant of VSV-G from the vesicular stomatitis virus New Jersey strain (VSV-G-NJ) and a VSV-G antibody (8G5F11) that only binds VSV-G of the Indiana strain, which we used throughout this

Please cite this article in press as: Zhang et al., Programmable Extracellular Vesicles for Macromolecule Delivery and Genome Modifications, Developmental Cell (2020), https://doi.org/10.1016/j.devcel.2020.11.007

work. As shown in Figure 1J, VSV-G-NJ is also capable of efficiently delivering Cre (Munis et al., 2018). Conversely, upon incubation with 8G5F11, Cre transfer by VSV-G was completely abolished while VSV-G-NJ mediated transfer was barely affected. These results demonstrate that Gectosome delivery requires VSV-G interaction with the cell membrane and subsequent fusion for efficient cargo release.

How does Gectosomal delivery compare with other dose-controlled delivery systems? Liposomes are well-established vehicles for the delivery of nucleic acids but are known to be not optimal for protein delivery (Colletier et al., 2002; Yu et al., 2019, 2015, 2018; Zelphati et al., 2001). To compare the delivery efficiency of Gectosomes with liposomes, we first quantified the amount of Cre encapsulated in Gectosomes using recombinant Cre as the standard for immunoblotting (Figure S2H). Next, we prepared liposomes encapsulating a defined amount of recombinant Cre using previously optimized methods (Yu et al., 2019, 2015, 2018) (Figure S2I). Approximately 510 nM of Cre delivered by liposomes is required to produce 19.3% of cells to switch. With Gectosomes, a similar effect is achieved with about 0.81 nM of Cre (Figures 1K, S2I, and S2J). Thus, based on the Cre amount delivered, Gectosomes showed ~630-fold higher delivery efficiencies than liposomes. These results demonstrate that Gectosomes outperform liposomes in delivering Cre into the nucleus, presumably due to better endosome escape or more robust fusion (Albertini et al., 2012).

Functional Separation of Gectosomes from Exosomes

Although exosomes and Gectosomes differ in size and intracellular origin, both can load protein or nucleic acid cargos from producer cells and transfer them to target cells. We wondered whether the active cargo-loading strategy we developed for Gectosomes could be extended to exosomes. To test this notion, we inserted GFP11 to the C-terminal of CD9 and CD81; two protein markers are known to be present on the surface of exosomes (Raposo and Stoorvogel, 2013). Next, we co-expressed CD9-GFP11, CD81-GFP11, or VSV-G-GFP11 together with Cre-GFP1-10 in 293T cells to produce exosomes and Gectosomes (Figure 2A). Successful and robust reconstitution of the GFP signal was seen with all three pairs (Figure 2B). NTA of the conditioned media from the transfected cells confirmed that fluorescent EVs were produced at comparable levels (Figure 2C). While Gectosomes triggered a robust color switch (~86%) consistent with the transfer of Cre, less than 3% of cells were switched with CD9 EVs, and even lower efficiency of the switch with CD81 EVs was observed (0.4%) when similar numbers of fluorescent particles were applied (Figure 2D). Although both the loading strategy and production of fluorescent EVs are comparable between types of encapsulation, intracellular delivery efficiency is vastly different. This result suggests that CD9- or CD81-containing vesicles, presumably exosomes, are functionally distinct from Gectosomes for protein transduction.

Differentiating and classifying EVs remains a major challenge due to their heterogeneity in size and contents. If Gectosomes and exosomes are separable entities in their biogenesis, we would expect that perturbing the biogenesis of one entity should have minimal effect on the other. Previous studies showed that acute Ca^{2+} spikes stimulate exosome release in a Munc13-4-dependent manner and that knockdown of this protein significantly inhibited exosome secretion (Messenger et al., 2018). To test whether Munc13-4 differentially regulates Gectosome and exosome production in 293T cells, we selected stable cell pools expressing *Munc13-4* sgRNA and SpCas9 by lentiviral infection. Western blotting showed a partial loss of Munc13-4 expression in the selected cell pool (Figure 2E). In agreement with previous results, significant reductions in CD9, GW130, and GAPDH levels were observed in supernatant collected from *Munc13-4*-edited cells (Figure 2E), consistent with inhibition of exosome release. To determine whether *Munc13-4* perturbation also affected the secretion of both endogenous and exogenous CD9, we transiently co-transfected CD9-GFP11 and Cre-GFP1-10 into wild-type and *Munc13-4*-edited cells (Figure S3A). The expression of CD9-GFP11/Cre-GFP1-10 in wild-type cells was indistinguishable from expression in edited cells (Figures 2F and S3A). However, the number of GFP-positive CD9 exosomes from *Munc13-4*-edited cells was ~2-fold lower than from wild-type cells, as measured by FACS (Figures 2G and S3B). Thus, the depletion of *Munc13-4* causes intrinsic defects in the production of CD9-positive exosomes. To investigate Gectosome production, we transfected wild-type and *Munc13-4*-edited cells with VSV-G-GFP11 and BlaM-Vpr-GFP1-10. We found that fluorescent Gectosome secretion is comparable between these two cell lines (Figure 2H), and the efficiency of BlaM delivery to HeLa cells is also indistinguishable between the Gectosomes collected from those two producer cell lines, indicating that Gectosome production is independent of Munc13-4 (Figure 2I).

We further investigated whether Gectosomes can be separated from exosomes biochemically. Using magnetic beads coated with an anti-CD9 antibody, we depleted CD9 exosomes from VSV-G-GFP11/Cre-GFP1-10 Gectosomes and measured the remaining Gectosome activity following serial dilutions (Figures S3C–S3E). Only a small reduction in Gectosome activity was observed (Figures S3C and S3D), suggesting that the bulk of Gectosome activity is not significantly affected by the removal of CD9 exosomes.

Finally, we also tested the effect of GW4869, a potent neutral sphingomyelinases inhibitor known to block exosome biogenesis (Menck et al., 2017), on Gectosome production in the producer cells. Following mock and co-transfection of VSV-G-GFP11/Cre-GFP1-10, 293T cells were treated with GW4869 (10 μM) to assess the effect on CD9 production and Gectosome activity. As expected, GW4869 reduced CD9 exosome secretion in both mock and Gectosome-producing cells (Figure S3F), whereas the activity of VSV-G-GFP11/Cre-GFP1-10 was not affected (Figure S3G). This result further supports that Gectosomes and exosomes are functionally separable.

Purification, Quantitation, and Mathematical Modeling of Gectosomes

Using a well-established protocol developed for purification of exosomes (Kowal et al., 2016), we tried to separate Gectosomes from other EVs by differential ultracentrifugation (UC) and flotation in a density gradient. While this procedure effectively enriches exosomes as measured by CD9 and GM130, Gectosomes components are also enriched in 100-K UC sediments (Figure S4A). To solve this problem, we developed a scalable purification protocol for Gectosomes that involves four major steps (Figure 3A). After two differential centrifugation steps, we applied

Please cite this article in press as: Zhang et al., Programmable Extracellular Vesicles for Macromolecule Delivery and Genome Modifications, Developmental Cell (2020), https://doi.org/10.1016/j.devcel.2020.11.007

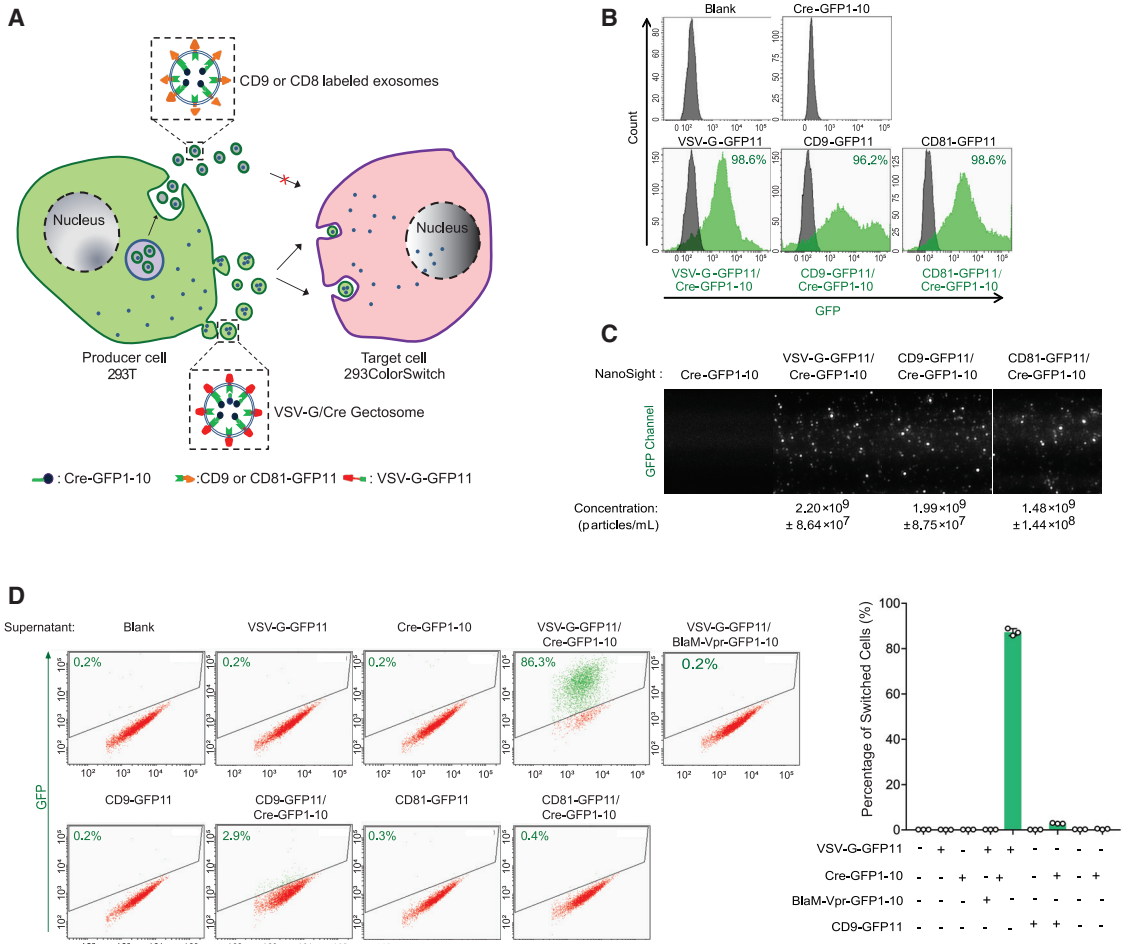

Figure 2. Functional Separations of Gectosomes from Exosomes

(A) Schematic diagram of experimental design (not to scale).

(B) Representative histograms of flow cytometric analysis of 293T cells transiently transfected with plasmids as shown.

(C) Nanoparticle tracking analysis of EVs from culture supernatants of 293T cells transfected with the indicated plasmids. Data are mean ± SD (n = 3).

(D) Flow cytometric analysis of 293ColorSwitch cells incubated with Cre Gectosomes, BlaM Gectosomes, or CD9/CD81-labeled exosomes. Representative dot plots and the quantification of switched cells are reported (mean ± SD, n = 3).

(E) Western blot of Munc13-4, CD9, and GW130 in wild-type and *Munc13-4* knockout 293T cells.

(F) Flow cytometric analyses of the transfection efficiency of CD9-mCherry plasmid in wild-type and *Munc13-4* knockout 293T cells.

(G) Nanoparticle tracking analysis of the percentage of CD9-GFP11/Cre-GFP1-10-positive exosomes secreted from wild-type and *Munc13-4* knockout 293T cells.

(H) Nanoparticle tracking analyses of the concentrations of BlaM Gectosomes secreted from wild-type and *Munc13-4* knockout 293T cells.

(I) Flow cytometric analysis of CCF2 cleavage in HeLa cells transduced with BlaM Gectosomes from *Munc13-4* knockout or wild-type 293T cells. Data for (F)–(I) are mean ± SD (n = 3). Statistical significance was assessed using Student's t test. **p < 0.001; n.s., not significant.

See also Figures S3 and S4.

Please cite this article in press as: Zhang et al., Programmable Extracellular Vesicles for Macromolecule Delivery and Genome Modifications, Developmental Cell (2020), https://doi.org/10.1016/j.devcel.2020.11.007

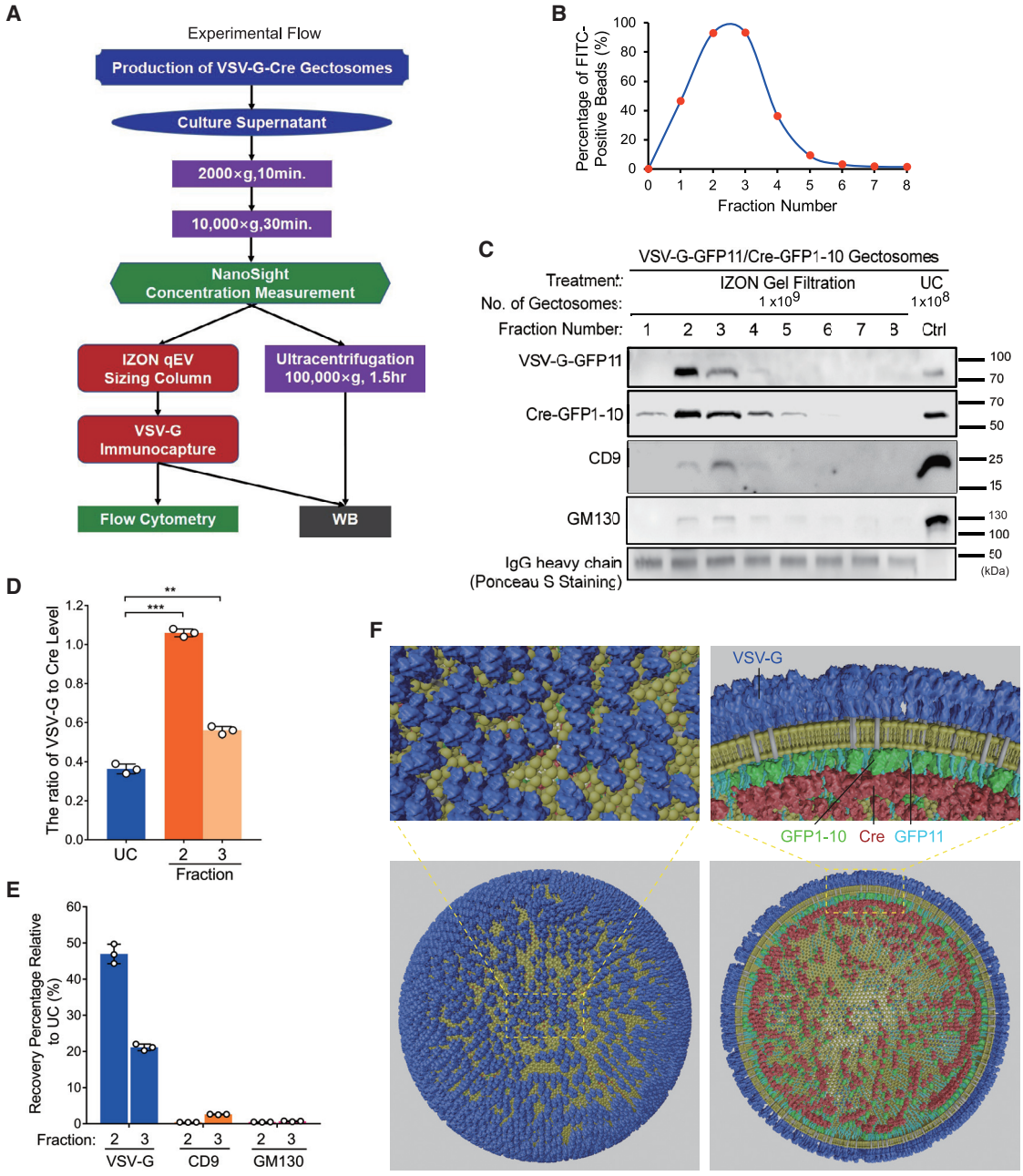

Figure 3. Purification, Quantitation, and Mathematical Modeling of Gectosomes

(A) The flowchart of the Gectosome purification procedure.

(B and C) Flow cytometric and western blotting analysis of Cre Gectosome fractions off the IZON qEVoriginal column. EVs pre-cleaned by 10,000 × *g* centrifugation were loaded onto the IZON qEVoriginal column. The fractionations 1–8 were incubated with VSV-G antibody crosslinked magnetic beads. The beads were washed, and a portion of the beads was subjected to flow cytometric analysis (B) and western blotting analysis (C). UC denotes samples prepared by ultracentrifugation (100,000 × *g*, 90 min).

(D) The ratios of VSV-G-GFP11/Cre-GFP1-10 in factions 2 and 3 or UC were calculated based on band intensities in (C).

(E) The percentages of VSV-G-GFP11, CD9, and GM130 in the fractions 2 and 3 versus the corresponding proteins in the UC sample were calculated based on relative band intensity in (C).

(F) 3D mathematical modeling of the Cre Gectosome. The left panels show an outside view of a modeled prototypical Gectosome and its local zoom-in view. The right panel shows the middle intersection view of a Gectosome and its local zoom-in view. This 3D model is illustrated according to the space-filling of 5,620 VSV-G-GFP11 molecules and 933 Cre-GFP1-10 molecules in a Cre Gectosome. The numbers of proteins of interest in this model are derived from the quantitative western blotting results in Figures S4B–S4D and 3C. Data are mean ± SD (n = 3); statistical significance for (D) was assessed using Student's t test (**p < 0.01; ***p < 0.001). UC, ultracentrifugation.

See also Figure S4.

Please cite this article in press as: Zhang et al., Programmable Extracellular Vesicles for Macromolecule Delivery and Genome Modifications, Developmental Cell (2020), https://doi.org/10.1016/j.devcel.2020.11.007

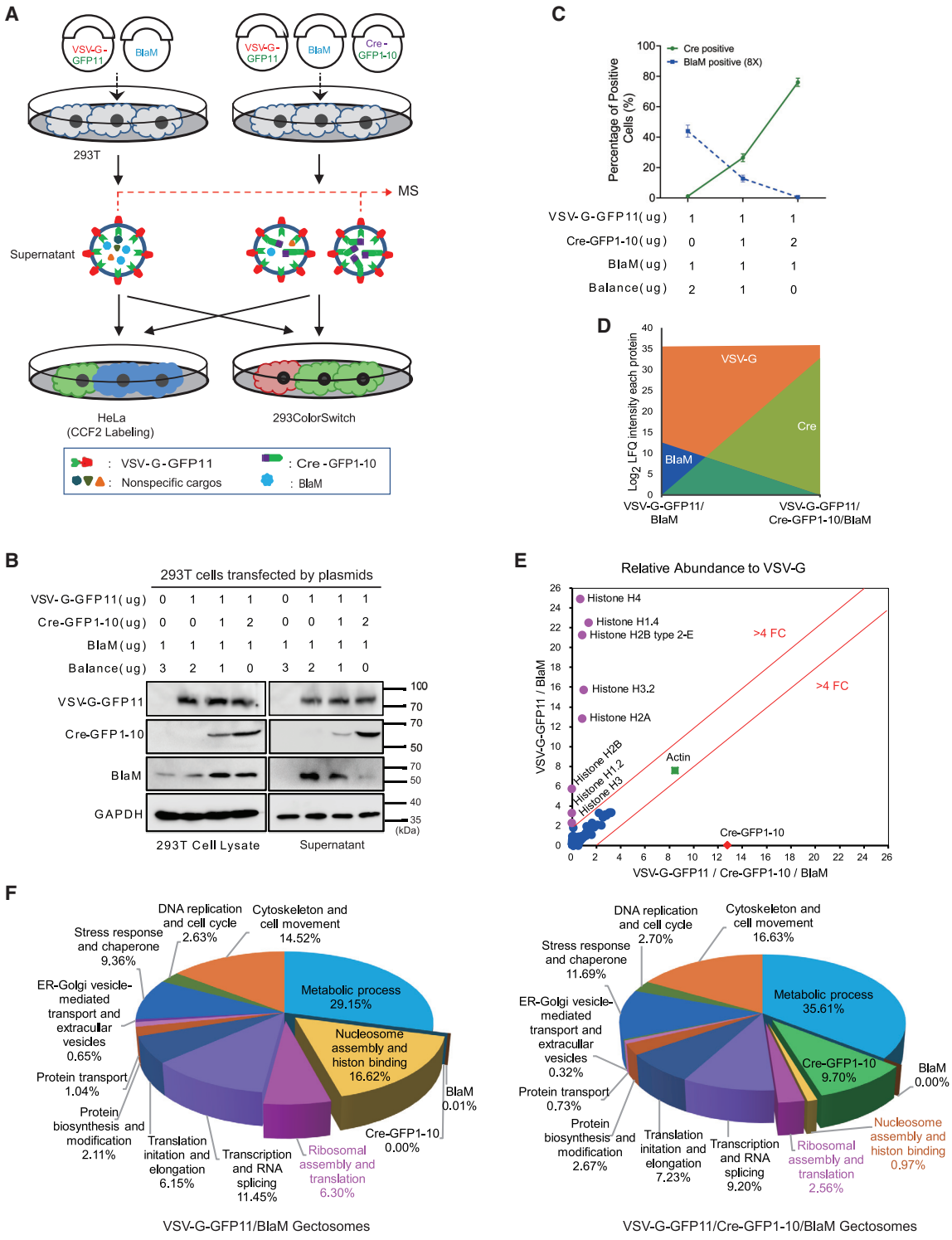

Figure 4. Active Loading of Gectosomes via the Split GFP System Reduces the Passive Incorporation of Cellular Proteins

(A) Illustration of the experimental design showing the competitive encapsulation of cargo protein of interest into Gectosomes. Cre-GFP1-10 is the cargo protein of interest, and untagged BlaM is used as a proxy for measuring non-specific incorporation of proteins into Gectosomes.

(B) The expression of VSV-G-GFP11, Cre-GFP1-10, and BlaM proteins in 293T cells lysates (left panel, ~10^5 cells/lane) transfected with plasmids shown, and ultracentrifugation concentrated supernatants (right panel, ~8 × 10^9 particles/lane). Balance refers to non-specific DNA that was included to ensure the same amount of total input DNA.

(legend continued on next page)

Please cite this article in press as: Zhang et al., Programmable Extracellular Vesicles for Macromolecule Delivery and Genome Modifications, Developmental Cell (2020), https://doi.org/10.1016/j.devcel.2020.11.007

the resuspended 10K pellet on a qEV 70 nm (IZON) size SEC column and collected the fractions with FITC fluorescence. Magnetic beads with immobilized anti-VSV-G 8G5F11 antibody were used to capture the Gectosomes before final elution with low pH glycine. Shown in Figures 3B and 3C, most Gectosomes are present in the second and third qEV fractionations based on the fluorescence intensity and captured VSV-G-GFP11 and Cre-GFP1-10 by western blot. VSV-G versus Cre ratios in fraction 2/3 are increased dramatically compared with that of the UC sample (Figures 3C and 3D). While 100,000 × g ultracentrifugation fractionation results in highly enriched CD9 and GM130 (Figures S4A and 3C), IZON fractionation followed by immunocapture significantly decreases CD9 and GM130 but increases VSV-G in fractions 2 and 3 when compared with the corresponding proteins in UC samples (Figures 3C and 3E). This result suggests that our purification protocol is very effective in removing exosomes, while the residual amount of CD9 in the Gectosome fractions may come from the cell surface. This result also further supports a biochemical distinction between Gectosomes and exosomes.

To develop a 3D molecular model for a prototypic Gectosome, we first performed quantitative measurements of VSV-G and Cre in Gectosomes by immunoblotting using purified recombinant proteins as standards (Clarke et al., 2006; Clarke and Liu, 2010). The number of VSV-G-GFP11 and Cre-GFP1-10 is estimated at ~5,620 and ~933 molecules respectively per gectosome (Figures S4B–S4D). We constructed a 3D molecular model of a Gectosome filled with VSV-G, sfGFP, and Cre from their known molecular structures in PDB using 3D software Blender (https://www.blender.org) (Figures S4E and 3F). The model derives from the "best guess" numbers (Table S1 and STAR Methods) and needs to be refined when better analytical techniques become available. Nevertheless, an average gectosome model can guide our understanding of Gectosomes. In this model, Cre-GFP1-10 occupies about ~13% of the total lumen space and spatially fills ~41% the hollow sphere beneath the inner membrane due to its strong association with VSV-G-GFP11 (K_d<1 nM) (Cabantous et al., 2005; Köker et al., 2018) (Figure S4E and STAR Methods). The modeling results prompted us to investigate what other proteins may be present in Gectosomes and whether active loading of Cre-GFP1-10 deters the recruitment of certain cellular proteins.

Active Loading of Gectosomes via the Split GFP System Reduces Passive Incorporation of Cellular Proteins

We considered two possible models of cargo encapsulation in Gectosomes with the split GFP system. One model is that active loading of Cre-GFP1-10 simply adds to the repertoire of existing proteins in Gectosomes without changing its baseline composition. A second competing model is the encapsulation of Cre-GFP1-10 remodels Gectosomes by specifically outcompeting other cellular proteins. The second model predicts that an increasing amount of Cre-GFP1-10 in Gectosomes will reduce non-specific incorporation of a cytosolic reporter protein. To test this model, we transfected 293T cells with the same amount of VSV-G-GFP11 while varying the ratio of input Cre-GFP1-10 (specific protein) to BlaM (non-specific protein). Gectosomes were collected and incubated with either 293ColorSwitch or HeLa cells to measure the activity of these two enzymes, respectively (Figure 4A). Supernatants and cell lysates were also blotted with relevant antibodies to verify the amount of Cre and BlaM in Gectosomes (Figure 4B). The increasing Cre-GFP1-10 lowers non-tethered BlaM in Gectosomes, which is corroborated by the activity of Cre and BlaM measured in two cell lines described above (Figure 4C).

To directly test the second model, we purified Gectosomes produced by co-transfection with VSV-G-GFP11 along with untethered BlaM with or without specific cargo protein Cre-GFP1-10 i.e., VSV-G-GFP11/BlaM (VB) versus VSV-G-GFP11/Cre-GFP1-10/BlaM (VCB) (Figure 4A). Since Gectosomes encapsulate untethered BlaM protein, we reasoned that it could serve as a proxy for non-specific recruitment. Harvested Gectosomes were immunocaptured with anti-VSV-G agarose beads and subsequently eluted off the beads with 1% SDS buffer. An equal amount of input proteins in duplicates were digested with trypsin and analyzed by label-free quantification (LFQ) mass spectrometry (MS). The values of Log_2 LFQ intensity of all detected proteins are ranged from around 21 to 35, which means the data quality is suitable for further analysis (Figure S4F; Table S2). We first compared the Log_2 LFQ intensity values of the known proteins (VSV-G and BlaM) shared in these two Gectosome samples (Figure 4D; Table S2). The number of VSV-G peptides detected (27 versus 26) and the Log_2 LFQ intensity value (35.58 versus 35.95) are comparable, suggesting the equivalent amounts of VSV-G-GFP11 in two Gectosomes. Three peptides of BlaM (Log_2 LFQ intensity is 12.6) were detected in VB Gectosomes, in contrast, none was detected in VCB Gectosomes. This result suggests that BlaM is excluded in the presence of Cre-GFP1-10, which supports the results of the experiment shown in Figures 4B and 4C.

Next, we quantified the endogenous proteins identified in both Gectosome samples (Table S2). MS peptide, intensity, and LFQ data show that VCB Gectosomes carry less randomly packaged

(C) Flow cytometric analysis of 293ColorSwitch cells and CCF2-loaded HeLa (BlaM-positive) cells that were transfected using plasmids as indicated. Since untethered BlaM in Gectosomes is very low, the supernatant was concentrated 8-fold by ultracentrifugation before incubation with HeLa cells. Data are mean ± SD (n = 3) and are representative of three individual experiments.

(D) MS analysis of immunoaffinity-purified VSV-G-GFP11/BlaM and VSV-G-GFP11/Cre-GFP1-10/BlaM Gectosomes. The graph shows the Log_2LFQ intensity of VSV-G, BlaM, and Cre in these two types of vesicles.

(E) Label-free quantitative MS analysis of the abundances of identified proteins relative to VSV-G in the indicated Gectosomes. The abundance value of each cargo protein is shown in Table S2. For data visualization, the abundance of VSV-G-GFP11 was assigned as 100, and the relative abundances of the rest of the proteins identified were calculated according to their Log_2LFQ intensity values relative to VSV-G-GFP11. Protein abundances in relative values to VSV-G as determined by MS of VSV-G/Cre-GFP1-10/BlaM Gectosomes (x axis) compared with VSV-G/BlaM Gectosomes (y axis). Red lines represent the gate of 4-fold change (FC).

(F) Pie charts showing the volume distribution of proteins in each GO category in the indicated Gectosomes by a combination of experimental and modeling analysis.

See also Figure S4.

Please cite this article in press as: Zhang et al., Programmable Extracellular Vesicles for Macromolecule Delivery and Genome Modifications, Developmental Cell (2020), https://doi.org/10.1016/j.devcel.2020.11.007

endogenous proteins (Figure S4G). We plotted the Log_2 LFQ intensity values of all detected proteins in both samples (Figure S4H). There are about 323 proteins shared between the two samples (Figure S4H). Of these, 27 proteins appear to be more abundant in the VB sample. Additionally, 453 proteins were found only in the VB Gectosomes and 41 proteins were found only in the VCB Gectosomes. Overall, VB Gectosomes contain more diverse set of proteins than VCB Gectosomes do, even though both species contain an almost identical amount of VSV-G-GFP11.

The MS data were further analyzed in the context of our 3D molecular model. First, we ranked proteins identified in two Gectosomes by their abundance relative to VSV-G-GFP11 based on the LFQ intensity. The result showed a dramatic reduction of histones in the presence of Cre-GFP1-10 (Figure 4E). Second, we estimated the molecular volume (partial specific volume) of the lumen proteins from their molecular weight using a simplified biophysical equation (Erickson, 2009). This approximation allowed us to compute the packing of Gectosomes in response to active loading. We summed up the total volume of lumen proteins in each Gectosome scaled to their relative abundance to VSV-G-GFP11. The total calculated volume of these proteins accounts for ~20% of our 3D molecular model's theoretical lumen volume for VB and VCB Gectosomes (Table S3). Plotting the proteins' volume distribution according to their GO classifications shows that major differences between VCB and VB Gectosome's cargo composition are the nucleosomal and ribosomal proteins (Figure 4F), which agrees with the abundance changes described above (Figure 4E). Taken together, these results support a model that active Gectosome loading via split GFP outcompetes non-specific encapsulation of cellular proteins and thereby reduces the heterogeneity of Gectosomes.

Gectosomes Can Deliver Versatile Cargos into Target Cells and Program Gene Expression

Can Gectosomes be engineered to deliver gene modifying functionality to target cells? To address this question, we designed Gectosomes that encapsulate AGO2 (Hammond et al., 2001) and SaCas9 (Ran et al., 2015). Flow cytometry, confocal microscopy, and western blot analyses confirmed that these proteins formed complexes with VSV-G-GFP11, mediated by split GFP, and were released from cells (Figures S5A–S5C). To test whether Gectosomes can package and deliver RNA-interfering functionality to target cells, we used a co-transfection system where cells received Gectosomes containing GFP1-10 fused to AGO2 and the shRNA targeting the mitochondrial kinase PINK1. AGO2 is a component of the RNA-induced silencing complex that binds and unwinds the small interference RNA duplex (Hammond et al., 2001). The resulting vector, AGO2-GFP1-10, was co-transfected with VSV-G-GFP11 into 293T cells. Another RNA-binding protein, ELAV/HuR, was used as a negative control in this experiment. Resulting Gectosomes were then collected for testing. PTEN induced kinase 1 (PINK1) is a kinase that recruits the E3 ubiquitin ligase Parkin to mitochondria in response to the oxidative phosphorylation uncoupler, CCCP (Narendra et al., 2010; Zhang et al., 2014), resulting in acute mitophagy. As expected, in HeLa-Venus-Parkin-RFP-Smac cells without Gectosomes, Venus-tagged Parkin localized diffusely in the cytosol of unstimulated cells and relocated to mitochondria upon CCCP treatment (Figure 5A). However, cells exposed to Gectosomes carrying PINK1 shRNA showed reduced Parkin accumulation on the mitochondrial surface in response to CCCP. This blockage of Parkin recruitment was observed only with AGO2/shPINK1 Gectosomes and not the ELAV1/shPINK1 Gectosomes; knockdown of PINK1 by AGO2/shPINK1 Gectosomes was confirmed with real-time PCR analysis and immunoblotting (Figures 5C and 5D). The imperfect correlation between PINK1 knockdown and Parkin localization could result from the off-target effect associated with each shRNA delivery method (Figures 5B and 5C). Nevertheless, these results demonstrate that Gectosomes can be programed with RNA-interfering complexes to inactivate genes of interest selectively.

To investigate whether these Gectosomes can deliver a competent gene-editing complex capable of making targeted changes to target cells' genomes, we collected Gectosomes from 293T cells made by co-transfecting VSV-G-GFP11 and SaCas9-GFP1-10, with or without PINK1 sgRNA. These Gectosomes were incubated with HeLa cells expressing Venus-Parkin. Without PINK1 sgRNA, SaCas9 Gectosomes did not affect Venus-Parkin mitochondrial recruitment. In contrast, cells exposed to SaCas9/PINK1 sgRNA Gectosomes showed a 40% reduction in the number of cells positive for Parkin recruitment (Figures 5E and 5F). This was accompanied by a partial reduction of PINK1 expression as determined by western blotting (Figure 5G). The incomplete effect on PINK1 loss is likely due to the fact that not all gene-editing events cause loss of function in a heterogeneous cell population. In addition to HeLa-Venus-Parkin-RFP-Smac cells, we also incubated SaCas9/PINK1 sgRNA Gectosomes with HeLa cells stably expressing PINK1-EGFP and observed partial loss of GFP signal by flow cytometry and western blot (Figures S5C–S5E). Sequencing analysis of genomic DNA from edited cells showed variable size deletions near the sgRNA targeting site (data not shown). These results indicate that Gectosomes can be designed to encapsulate RNA interference or gene-editing machinery to alter gene expression.

CD47 Suppresses Gectosome Clearance by Macrophages

Circulating monocytes, macrophages, dendritic cells, and neutrophils remove dead cells, cell debris, exosomes, and ectosomes through phagocytosis (Barclay and Van den Berg, 2014). These phagocytic cells express signal regulatory protein α (SIRPα), which serves as a receptor for CD47, a transmembrane protein present in high levels in tumor cells and normal cells alike. Binding of CD47 to SIRPα triggers a "do not eat me" signal (Chao et al., 2012). Previous studies showed that the presence of CD47 on exosomes suppresses their depletion by phagocytosis, resulting in higher exosome levels in the blood (Kamerkar et al., 2017). In contrast, CD47 blockade with a nanobody (nb) A4 enhanced macrophage phagocytosis of tumor cells (Sockolosky et al., 2016). To test if the CD47-SIRPα system plays a role in Gectosome clearance by macrophages *in vitro*, we overexpressed Myc and GFP11-tagged mouse CD47 or CD47nb in 293T cells, along with the standard Gectosome components (Figure 6A). With this design, Gectosomes were generated with higher CD47 or CD47nb expression on their surfaces, along with VSV-G (Figure 6B). Without VSV-G-GFP11, CD47-Myc-

Developmental Cell
Technology

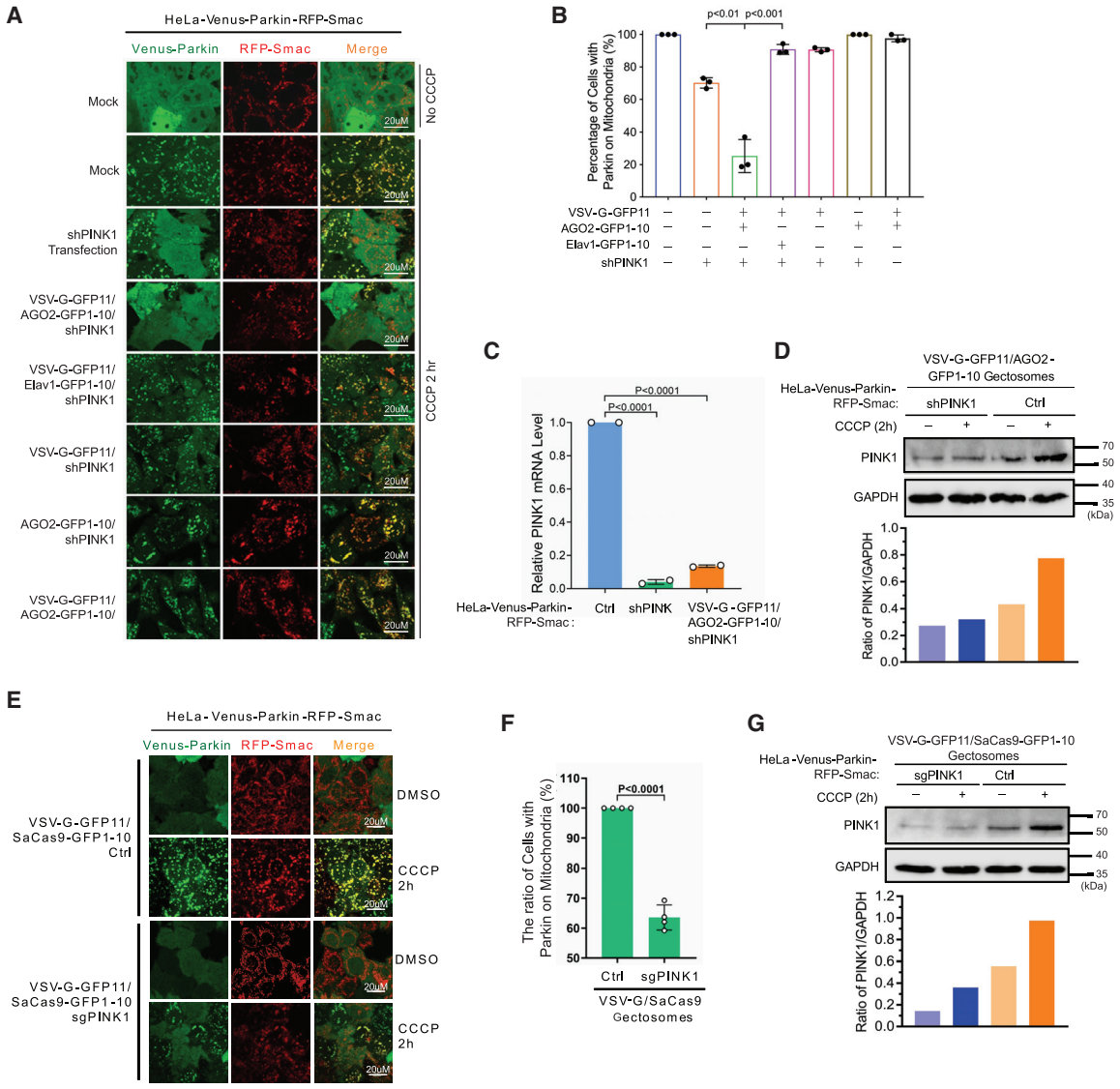

Figure 5. Gectosomes Can Deliver Versatile Cargos into Target Cells and Program Gene Expression

(A) Confocal images of HeLa-Venus-Parkin-RFP-Smac cells transduced with Gectosomes carrying the indicated cargo proteins or nucleic acids.

(B) Quantification of the percentage of cells with Parkin on mitochondria after 10-μM CCCP treatment for 2 h in (A). n >200 cells for each condition from 3 replicates. Data are mean ± SD (n = 3).

(C) The RT-qPCR analysis of the efficiency of *PINK1* knockdown in cells treated as indicated. The expression levels of PINK1 were normalized to that of GAPDH. Results are shown as the averages ± standard error of the mean from two independent replicates (n = 2).

(D) Western blotting analysis of PINK1 protein in HeLa-Venus-Parkin cells treated as indicated.

(E) Confocal images of HeLa-Venus-Parkin-RFP-Smac cells transduced with SaCas9/sgPINK1 Gectosomes or SaCas9/sgCtrl Gectosomes.

(F) Quantitation of the percentage of cells showing Venus-Parkin accumulation on mitochondria with 10-μM CCCP for 2 h n >200 cells for each condition from three replicates. Data are mean ± SD (n = 3).

(G) Western blotting analysis of PINK1 protein in HeLa-Venus-Parkin-RFP-Smac cells treated as shown. The relative amount of PINK1 in (D) and (G) was quantified by densitometry. Statistical significance for (B), (C), and (F) was assessed using the Student's t test.

See also Figure S5.

GFP11 or CD47nb-Myc-GFP11 cannot transduce BlaM-Vpr-GFP1-10 to target cells (Figures 6C and S6A). Next, we incubated control, CD47, and CD47nb Gectosomes containing BlaM-Vpr-GFP1-10 with mouse RAW 264.7 macrophages for 3 or 6 h. The supernatants were recovered after incubation, and BlaM activity assays measured the amount of Gectosomes remaining in the media. RAW 264.7 cells depleted approximately 25% and 70% of the control Gectosomes after 3 and 6 h (Figure 6D). In contrast, only 10% and 50% of CD47 Gectosomes were depleted, whereas 70% and 80% of CD47nb Gectosomes were removed from the media. Gectosome depletion was also confirmed by measuring the amount of GFP fluorescent particles

Please cite this article in press as: Zhang et al., Programmable Extracellular Vesicles for Macromolecule Delivery and Genome Modifications, Developmental Cell (2020), https://doi.org/10.1016/j.devcel.2020.11.007

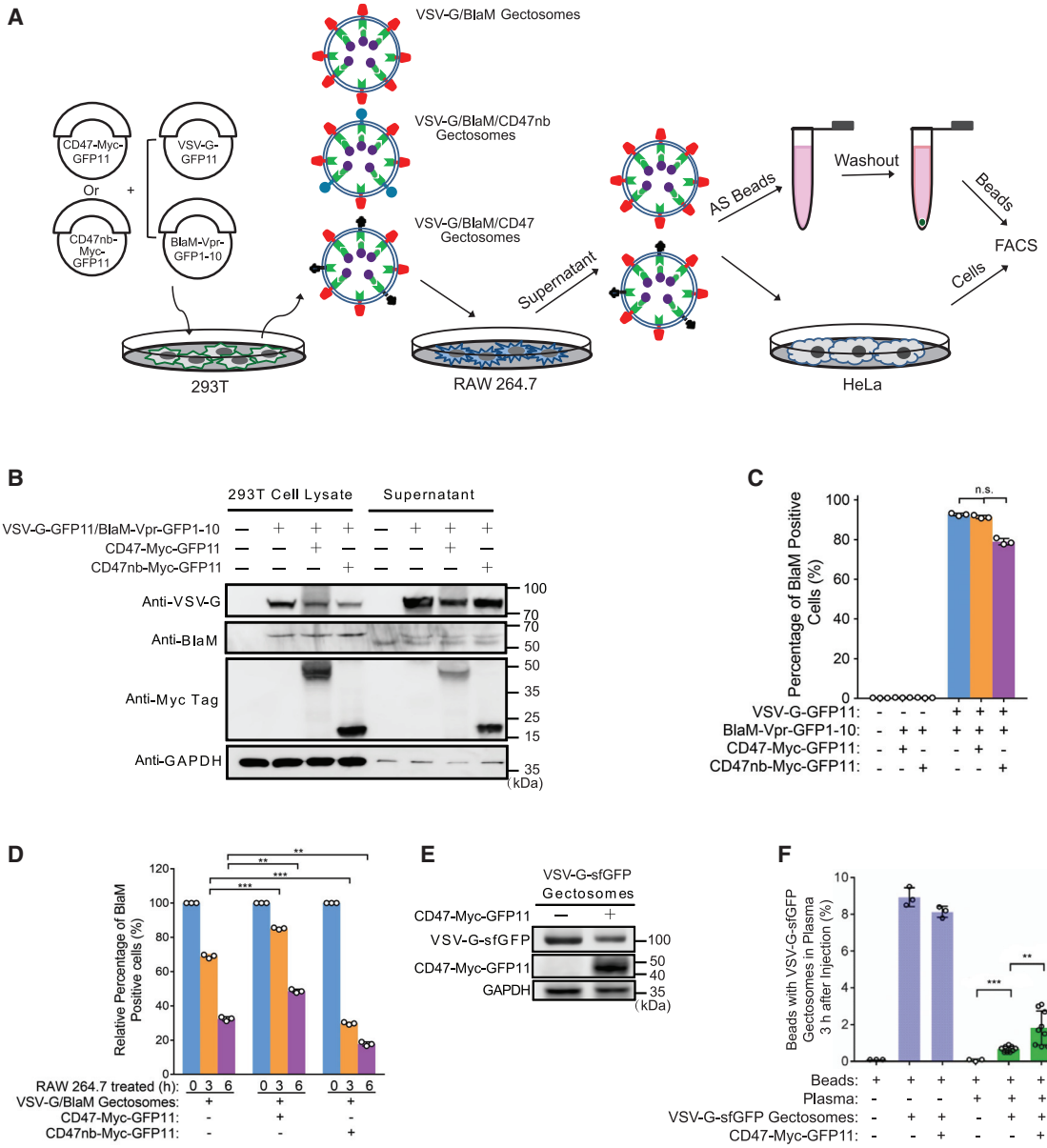

Figure 6. CD47 Suppresses Gectosome Clearance by Macrophages

(A) Schematic illustration of the experimental procedure for evaluating the effect of CD47 on Gectosome clearance.

(B) Western blotting analysis of cargo proteins in 293T cells and released Gectosomes.

(C) Effect of CD47 or CD47nanobody expression on the efficiency of Gectosome delivery of BlaM to HeLa cells. CCF2-loaded HeLa cells were incubated with VSV-G-GFP11/BlaM-GFP1-10 Gectosomes (with/without CD47-Myc-GFP11 or C47nb-Myc-GFP11 expression) and analyzed by flow cytometry. Data are mean ± SD (n = 3) and are representative of two individual experiments.

(D) Measuring Gectosome depletion by RAW 264.7 cells. BlaM Gectosomes (with/without CD47 or C47nanobody co-expression) (2 mL, ~2 × 10^8/mL) were incubated with RAW 264.7 macrophage cells (~10^6 cells/well in 6-well plate) for indicated time (0, 3, 6 h). After incubation, supernatants were retrieved by centrifugation at 1,000 rpm for 10 min to remove RAW 264.7 cells. Subsequently, the retrieved supernatants (2 mL) were incubated with HeLa cells (~3 × 10^5 cells/well in 6-well plate) for 16 h, and then cells were loaded with CCF2-AM before they were harvested for flow cytometric analyses. The percentage of BlaM-positive cells was normalized to 0-h incubation. Data are mean ± SD (n = 3) and are representative of two individual experiments. Statistical significance was assessed using the Student's t test (**p < 0.01; ***p < 0.001).

(E) Western blotting analysis of the proteins in Gectosomes collected from supernatants of 293T cells transfected with VSV-G-sfGFP with/without CD47-Myc-GFP11.

(F) The levels of VSV-G-sfGFP Gectosomes in the mouse blood circulation 3 h after intravenous injection. Approximately 10^9 VSV-G-sfGFP Gectosomes resuspended in 150 μL PBS were injected per mouse. Fluorescent Gectosomes in plasma were collected by aldehyde sulfate beads as described in

(legend continued on next page)

Please cite this article in press as: Zhang et al., Programmable Extracellular Vesicles for Macromolecule Delivery and Genome Modifications, Developmental Cell (2020), https://doi.org/10.1016/j.devcel.2020.11.007

left in the supernatants after macrophage exposure (Figure S6B). The effect of CD47 on Gectosome depletion by macrophage is not reporter specific, as Cre Gectosomes exhibit similar depletion trends (data not shown).

To test if CD47 suppresses Gectosome clearance in circulation *in vivo*, 4–6-week female BALB/c mice were injected intravenously with VSV-G-sfGFP Gectosomes, produced with or without CD47 (Figure 6E). The levels of fluorescent Gectosome particles in circulation 3 h post-injection were measured by flow cytometry analysis of aldehyde sulfate beads bound to the Gectosomes in mouse plasma. VSV-G-sfGFP Gectosomes with CD47 showed higher retention in circulation than those without CD47 (Figures 6F and S6C). Thus, these results demonstrate that the presence of CD47 on Gectosomes slows their removal by myeloid cells, and conversely, that perturbing CD47-SIRPα interactions accelerates their depletion.

PCSK9 Gene Editing in Mouse Livers through Systemic Gectosome Delivery of Gene-Editing Machinery

Previous studies have shown that AAV viral delivery of SaCas9 and a sgRNA targeting proprotein convertase subtilisin/kexin type 9 (*PCSK9*) to mouse liver cells results in a significant reduction of serum PCSK9 and total cholesterol levels (Ran et al., 2015). Given concerns about the sustained expression of SaCas9/sgRNA expression *in vivo*, we wished to determine whether Gectosomes could induce gene editing in somatic tissues of animals through transient delivery of gene-editing machinery. To this end, we first confirmed the editing activity of the two validated sgRNAs targeting PCSK9 used in the previous studies (Ran et al., 2015) in MEF cells using Gectosome delivery (data not shown).

To test whether Gectosome could deliver SaCas9/mPCSK9 sgRNA *in vivo*, we injected Gectosomes (10^9 per mouse per injection) carrying SaCas9/mPCSK9 sgRNA to BALB/c mice on days 0, 2, and 4. The control group was injected with PBS. Serum PCSK9 and LDL cholesterol levels were measured in blood samples collected on the indicated days (Figures S7A and S7C). As early as 14 days after the initial injection, serum PCSK9 levels were significantly lower than those of the control groups (Figure S7A). This observation was corroborated by immunoblotting for PCSK9 in mouse liver tissues (Figure S7B). The serum LDL cholesterol levels also correlated with the decline of serum PCSK9 (Figure S7C). This result suggests that gectosomal delivery of the SaCas9 gene-editing complex is effective in lowering PCSK9 expression in mouse livers.

Next, we set out to test whether CD47 can promote Gectosome delivery efficiency *in vivo* by adding two additional groups: SaCas9 with Rosa26 sgRNA Gectosomes and CD47/SaCas9/mPCSK9 sgRNA Gectosomes (Figure 7A). The first one serves as the non-targeting control as Rosa26 sgRNA has been used in previous studies (Ran et al., 2015). The CD47 group was included based on our *in vitro* results showing reduced Gectosomes clearance by CD47. Similar to what we observed in the initial study, animals treated with SaCas9/mPCSK9 sgRNA Gectosomes showed a statistically significant reduction in both PCSK9 and LDL from the control with Rosa26 sgRNA (two-way ANOVA test) (Figures 7B–7D). The decline of LDL cholesterol levels in all groups between day 14 and day 21 may be caused by procedure-induced stress. The CD47 group showed consistently lower PCSK9 and LDL cholesterol levels and higher statistical significance from the control group, although the difference between this group and that without CD47 was found to be not statistically significant. The dynamics of LDL cholesterol change were unknown, but their separation from the control groups was consistent. There were no significant differences in body weight changes during the experiment between the group of animals (Figure 7E), suggesting no general systemic toxicity associated with Gectosome injection. To further confirm the *PCSK9* mutations caused by SaCas9/mPCSK9-sgRNA Gectosomes, genomic DNA was extracted from liver tissue, followed by PCR and DNA sequencing analyses. The results show that both deletions and mutations can be detected in the Gectosome-treated group (Table S4), confirming that gene editing indeed occurred *in vivo* upon Gectosome delivery of SaCas9/PCSK9 sgRNA complex. Overall, these results support the potential of Gectosomes to deliver effective genome-editing machinery to animal tissues.

DISCUSSION

Here, we have developed a method for pharmacologically delivering bioactive proteins, RNA-interfering machinery, and Cas9/sgRNA complexes *in vitro* and *in vivo*. Our method harnesses the unique properties of fusogenic Gectosomes and an active cargo-loading strategy to achieve the highly efficient delivery of macromolecules to the interior of mammalian cells. We found that active loading of Gectosomes via the split GFP system reduces vesicle heterogeneity by suppressing passive incorporation of cellular proteins, increases the specific activity of delivery, and enables purification of vesicles for cargo, thereby minimizing the undesirable effects bioactive contaminants.

Biologics designed for modulating intracellular targets are challenging to develop as therapeutics due to their reduced ability to penetrate the cell and endosomal membranes. With the development of genome-editing technologies and therapeutic nucleic acids, intense efforts are devoted to addressing these delivery issues. One of the most efficient approaches is the viral delivery of genetically encoded biologics. However, there are safety concerns about persistent exposure of the encoded agent in addition to immunogenic responses, or even oncogenic transformation (Nelson and Gersbach, 2016). As an alternative, liposomal agents have been developed and widely used for delivering nucleic acids from DNA to RNAi. While some liposomal gene therapies have advanced into clinical trials (Nelson and Gersbach, 2016), liposomal delivery of protein is generally less efficient and protein-specific due to the lack of dominant electrostatic property when compared with nucleic acids (Zuris et al., 2015). We compared these two methods and showed that liposomes require significantly more Cre protein (630-fold) to achieve the same biological effect (Figures 1K and S2H–S2J).

STAR Methods. These results are expressed as mean ± SD (n = 9) from three independent measurements for each mouse (n = 3 mice). Statistical significance for (C) and (F) was assessed using the Student's t test; n.s., not significant.
See also Figure S6.

Please cite this article in press as: Zhang et al., Programmable Extracellular Vesicles for Macromolecule Delivery and Genome Modifications, Developmental Cell (2020), https://doi.org/10.1016/j.devcel.2020.11.007

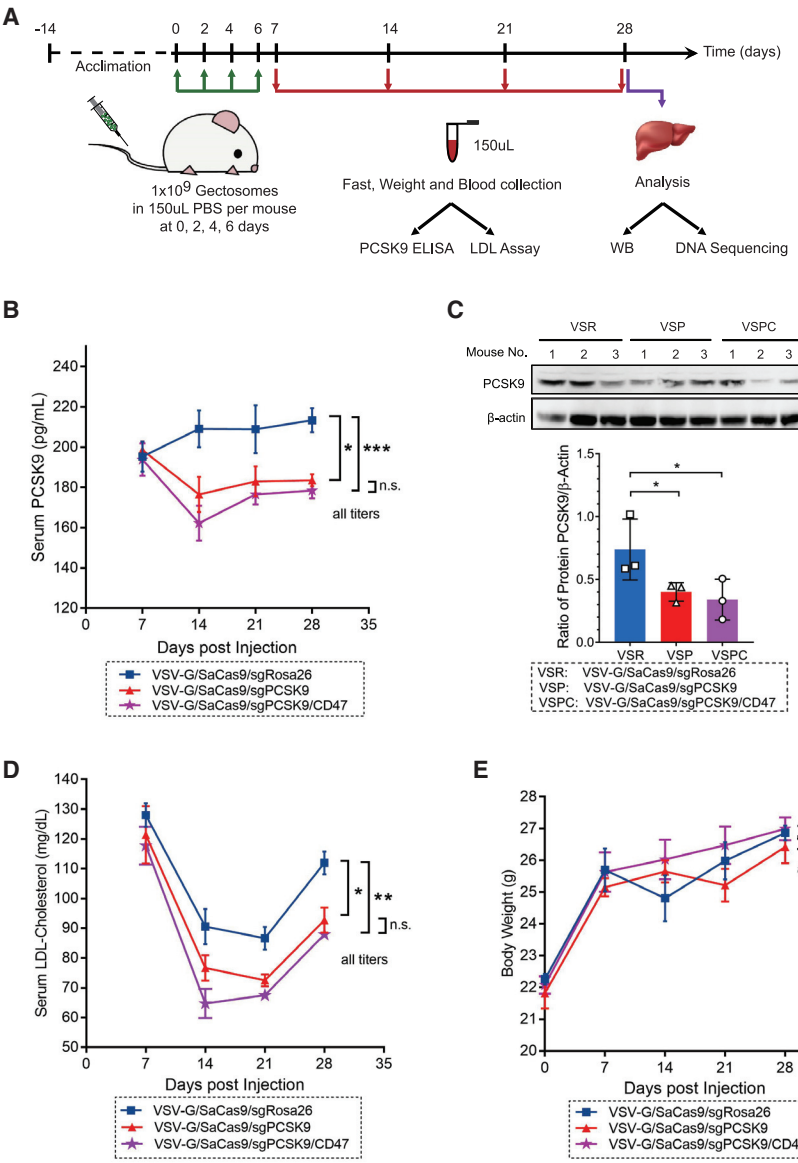

Figure 7. PCSK9 Gene Editing in Mouse Livers through Systemic Gectosome Delivery of Gene-Editing Machinery

(A) Schematic diagram of *in vivo* mouse experiment.

(B) Time course of serum PCSK9 levels in VSV-G/SaCas9/sgRosa26 group (n = 3 mice), VSV-G/SaCas9/sgPCSK9 group (n = 3 mice), and VSV-G/SaCas9/sgPCSK9/CD47 group (n = 4 mice). Each mouse received approximately 10^9 particles by tail vein injection four times at 48-h interval.

(C) Western blotting analysis of PCSK9 in liver tissue of mice harvested from the control and treated groups. For the SaCas9/sgPCSK9/CD47 group, three out of four mice were randomly selected. Quantitation of PCKS9 levels normalized to the loading control (β-actin) is shown below the blot.

(D) Time course of serum LDL cholesterol concentrations in mice injected with Gectosomes as in (B).

(E) The body weights of mice were not significantly different between the treatment groups. Arrows show the times of tail vein injection. Data are mean ± SEM; statistical significance for (C) was assessed using the Student's t test (*p < 0.05). Two-way ANOVA was used to determine the differences of all titers between groups in (B), (D), and (E) (*p < 0.05; **p < 0.01; ***p < 0.001).

See also Figure S7.

Several reasons may contribute to the high delivery efficiency of Cre by Gectosomes. First, VSV-G mediates efficient cellular entry of VSV particles by endocytosis via binding to the LDL-R family of receptors (Finkelshtein et al., 2013). Second, as a proficient fusion protein, VSV-G promotes the fusion of viral envelope with the early endosome membrane leading to the release of nucleocapsid into the cytoplasm (Albertini et al., 2012). It is highly probable that VSV-G performs a similar function in Gectosome uptake and cargo release. Third, due to the presence of chaperone proteins such as Hsp90 and Hsp70 in Gectosomes (Table S2) (Mangeot et al., 2011), Cre is less likely subjected to denaturation during encapsulation as reported with liposomes *in vitro* (Colletier et al., 2002). Therefore, VSV-G enables cargos encapsulated within Gectosomes to overcome the barriers of both the plasma and endosome membranes.

While the mechanism of VSV trafficking and nucleocapsid release in target cells is well characterized (Albertini et al., 2012), whether Gectosomes follow the same pathways to release the cargo remains unclear. We performed immunofluorescence microscopy of the time course of VSV-G-GFP11/Cre-GFP1-10 uptake in HeLa cells. The signals for VSV-G-GFP11 and Cre-GFP1-10 increase with the time of exposure (Figure S7G). VSV-G-GFP11 localizes primarily on vesicular structures and largely co-localizes with the reconstituted split GFP signal in vesicles and membrane but not in the nucleus. In contrast, the Cre-GFP1-10 signal is more diffused in the cytosol, membrane, nucleus, and vesicles (Figure S7G). Co-staining of VSV-G with Cre also shows that a significant fraction of the Cre signals, especially nuclear Cre, do not co-localize with VSV-G (Figure S7H). Cre-GFP1-10 shows a different time-dependent accumulation pattern from VSV-G-GFP11 intracellularly, suggesting Cre-GFP1-10 splits from VSV-G-GFP11 in the recipient cells. Gectosomes co-localize significantly with the early endosome marker EEA1 (Figure S7I), and a small fraction of Gectosome signals co-localize with the late endosome marker Lamp1 (Figures S7I and S7J). These results support a model that Gectosomes enter target cells via the endocytic route, and cargo can be released in the target cells. Two pathways for VSV cell entry have been proposed (Albertini et al., 2012). The prevailing pathway is that VSV-G mediates rapid fusion in early endosomes to release cargo to the cytosol. Another pathway involves VSV fusion with an internal vesicle inside multivesicular bodies (MVB). In the late endosome, the nucleocapsid is released to the cytosol through a back-fusion mechanism using the cellular

Please cite this article in press as: Zhang et al., Programmable Extracellular Vesicles for Macromolecule Delivery and Genome Modifications, Developmental Cell (2020), https://doi.org/10.1016/j.devcel.2020.11.007

fusion machinery (Le Blanc et al., 2005). Our data suggest that both pathways are possible for Gectosomes delivery, and the second pathway is particularly intriguing in light of the pH-sensitive nature of split GFP complementation (Cabantous et al., 2005). Future studies are necessary to address the detailed mechanism of Gectosome trafficking and cargo release.

Other groups have reported transduction of proteins or Cas9/sgRNA complex with VSV-G ectosomes (Campbell et al., 2019; Mangeot et al., 2011; Montagna et al., 2018). The key difference between our study and others is the strategy of cargo loading. Our approach enables direct tethering of cargo to VSV-G, while others use an artificial membrane protein known as CherryPicker to recruit cargo. We showed that the efficiency of cargo transfer with the tethered Cre-GFP1-10 to VSV-G-GFP11 is much higher than with the untethered one (~26-fold, Figures 1H and 1I). The direct fusion of cargo proteins to VSV-G frequently results in low efficiency of cargo delivery since VSV-G with fused cargo may interfere with proper trimer formation required for fusion (Dalton and Rose, 2001; Hung and Leonard, 2016). Rose and colleagues showed that in functional Vesicular stomatitis virus particles that encapsulate VSV-G-GFP, the ratio of wild-type VSV-G to VSV-G-GFP is 4.2:1(Dalton and Rose, 2001). Our mass spec data show the ratio of VSV-G-GFP11 to Cre-GFP1-10 is 6:1 in Gectosomes. Since the 16-aa GFP11 tag is less likely to perturb the fusion function of VSV-G, either the trimeric VSV-G-GFP11 or a heterocomplex consisting of 2 units of VSV-G-GFP11 and 1 unit of VSV-G–GFP11-cargo-GFP1-10 functions well in mediating Gectosome fusion. Our two-component Gectosome design with split GFP takes advantage of this property to enhance more specific cargo encapsulation and reduce non-specific cellular components.

Beyond genome editing, we further demonstrated that Gectosomes are more versatile in delivering a variety of biologics. With AGO2, it is possible to perform RNAi with Gectosomes (Figure 5). Although we mainly focused on delivering catalytic enzymes in this study, it is conceivable that Gectosome-based strategies could also be used to transduce other phenotype-modifying agents such as therapeutic antibodies, mRNA, transcription factors, or peptides. We also envision that Gectosomes can be used to deliver antigens and adjuvants for vaccine development. Since proteins delivered by Gectosomes are dose-dependent, rapidly released, and degraded intracellularly after 24–48 h, at least in the case of BlaM (data not shown), protein or RNA transduction mediated by Gectosomes is most likely transient in nature and dictated by the intrinsic half-lives of the transduced molecules. This feature is particularly desirable in therapeutic genome editing to minimize potential off-target editing that arises from the persistent expression of Cas9 in the genome. More experiments are needed to assess the consequences of long-term and multi-dose exposure to Gectosomes *in vivo*.

One potential limitation for a broader application of Gectosome delivery is the adaptive immunity to VSV-G or non-human cargo proteins. How quickly the adaptive immune system kicks in may dictate the types of applications for which Gectosomes can be utilized. While this may not be an issue for genome editing or vaccine development, delivering other therapeutic modalities may require multiple rounds of dosing over an extended period. One potential way to address this issue is to employ different subtypes of VSV-G (e.g., VSV-G-NJ in Figure 1J) to sidestep the adaptive immunity through alternate dosing of different pseudotyped Gectosomes. Another way of mitigating the immune response is to decorate Gectosomes with CD47. Since CD47 slows Gectosome depletion by phagocytic cells (Figure 6), we speculate that this strategy may reduce antigen presentation and delay the development of adaptive immunity. Finally, there could be endogenous VSV-G-like fusogenic proteins in human cells. Once the host fusogenic proteins are identified, future Gectosomes can be programed with such proteins to avoid adaptive immunity. We aim to address these issues in our future studies.

EVs are known to be heterogeneous. A long list of cytosolic and nuclear proteins has been found in VSV-G ectosomes by proteomics analysis (Mangeot et al., 2011). This heterogeneity constitutes a major barrier to developing therapeutics due to a lack of effective strategies to reduce heterogeneity. With an active cargo-loading approach using split GFP, we demonstrated that there is a significant reduction in both the number and the abundance of cellular proteins encapsulated in Gectosomes by quantitative MS analysis (Figure 4). A surprising result is that histones and nucleic-acid-binding proteins are selectively eliminated from Gectosomes with Cre-GFP1-10. These proteins are frequently found in exosomes and ectosomes (Haraszti et al., 2016; Jeppesen et al., 2019; Kowal et al., 2016; Mangeot et al., 2004). Since histones are highly basic proteins and may bind the inner plasma membrane via electrostatic interactions, we postulate that recruitment of Cre-GFP1-10 to the short cytoplasmic tail of VSV-G may occlude histones and other basic proteins from non-specific binding to the negatively charged inner membrane. As an additional effect, passive incorporation of nucleic acids (miRNA, mRNA, and DNA) could also be reduced. Future proteomics and NGS sequencing should help test these hypotheses. Regardless of the mechanisms involved, our active cargo-loading approach provides a means to reduce the heterogeneity of EVs and removes a considerable barrier to their development as delivery systems.

In summary, the Gectosome approach offers a blueprint for the intracellular delivery of biologics designed to modulate intracellular targets. Future improvements in this technology may enable the development of better therapeutics for a wide range of human diseases.

Limitations

Because Gectosomes use a split GFP to encapsulate a specific cargo, the functionality of the cargo of interest could be perturbed by the fusion with GFP1-10. It may be necessary to optimize the location of GFP1-10 within the fusion partner. The stability of cargo-GFP1-10 and its affinity to VSV-G-GFP11 may also affect the efficiency of cargo loading in producer cells and their release in target cells. The utility of Gectosomes to deliver intracellular therapeutics *in vivo* could be limited by adaptive immune response development to VSV-G. We may be able to address this issue by alternate dosing of Gectosomes pseudotyped with different variants of VSV-G subtypes or displaying a sufficient amount of CD47 to mitigate antigen presentation. Although we did not observe overt toxicity of Gectosome administration *in vivo*, many issues concerning safety, organ specificity, and pharmacology need to be addressed for developing broadly applicable therapeutic solutions.

STAR★METHODS

Detailed methods are provided in the online version of this paper and include the following:

- KEY RESOURCES TABLE
- RESOURCE AVAILABILITY
  - Lead Contact
  - Materials Availability
  - Data and Code Availability
- EXPERIMENTAL MODEL AND SUBJECT DETAILS
  - Animals
  - Cell Culture
- METHODS DETAILS
  - Gene Expression Constructs
  - Recombinant Protein Expression
  - Production of Gectosomes
  - Flow Cytometric Analysis of Gectosomes
  - Particle Size and Concentration Measurement by Nanoparticle Tracking Analysis (NTA)
  - Gectosome Release Assay
  - Immunoblotting Analysis
  - BlaM and Cre Protein Cellular Uptake Assays
  - Purification and Immobilization of the VSV-G Antibody
  - Isolation and Purification of Gectosomes
  - Fluorescence Microscopy
  - Negative Stain Transmission Electron Microscopy and Immunogold Labeling
  - Recombinant Cre Liposome Preparation
  - Mass Spectrometry Analysis
  - RNA Interference by Gectosomes
  - Genome Editing with CRISPR/Cas9 Gectosomes
  - Gectosome Clearance by Macrophage Cells
  - Gectosome Clearance in Mice
  - Genome Editing in Mice
  - Mathematical Modeling of Gectosomes
  - The Occupancy of VSV-G Proteins at the Surface of Gectosomes
- QUANTIFICATION AND STATISTICAL ANALYSIS
  - Image Analysis
  - Statistical Analysis

SUPPLEMENTAL INFORMATION

Supplemental Information can be found online at https://doi.org/10.1016/j.devcel.2020.11.007.

ACKNOWLEDGMENTS

We thank the anonymous reviewers for their thorough critiques of our manuscript and experimental recommendations. We thank Drs. Natalie Ahn, James Goodrich, Alexandra Whiteley, Melissa Stauffer, Mr. Christopher Ill, and Ms. Graycen Wheeler for critical readings of the manuscript. We thank Dr. Joseph Dragavon and the BioFrontiers Advanced Light Microscopy Core for their microscopy support, Dr. Garry Morgan for EM support, Drs. Thomas Lee and Chris Ebmeier of Central Analytical Mass Spectrometry Lab for their mass spectrometry support, Ms. Ishara Datta for the *Munc13-4* gene-editing vector, and Ms. Theresa Nahreini for technical assistance with cell sorting. We thank Dr. Neil King and Dr. Douglas Lyles for sharing BlaM, VSV-G expression vectors, and 8G5F11 hybridoma cells. This work was supported by grants from the National Institute of Arthritis and Musculoskeletal and Skin Diseases and the National Institute of General Medicine of the National Institutes of Health (NIH) (R01AR068254 and R01GM113141 to X.L.). L.C. was supported by a predoctoral training grant from the National Institute of General Medical Sciences (T32GM08759). The content is solely the responsibility of the authors and does not necessarily represent the official views of the NIH. The ImageXpress MicroXL imaging system was supported by NCRR S10RR026680, the BDAria cell sorter by S10OD021601, the Opera Phenix imaging system by S10OD025072, and the Thermo Q Exactive HF-X mass spectrometer and Ultimate 3000 RSLCnano system by NIH S10OD025267 from the NIH.

AUTHOR CONTRIBUTIONS

X.Z., Q.X., J.S., and X.L. conceived and designed the study. X.Z., Q.X., Z.L., L.C., C.W., and X.L. performed experimental studies. Z.Z. developed the mathematical model and performed the computational analysis. X.Z., Q.X., Z.Z., and X.L. wrote the manuscript. All authors discussed the results and contributed to the final manuscript.

DECLARATION OF INTERESTS

The University of Colorado Boulder currently holds the PCT patent for the use of Gectosome technology, with X.Z., Q.X., Z.L., and X.L. as inventors. X.L. is a co-founder, member of Board of Directors, and paid consulting CSO of OnKure Inc., which has no relationships or competing interests to this study. X.L. owns equity in OnKure Inc. Z.Z., C.W., L.C., and J.S. declare no competing interests.

Received: August 21, 2019
Revised: May 13, 2020
Accepted: November 4, 2020
Published: December 8, 2020

REFERENCES

Albertini, A.A., Baquero, E., Ferlin, A., and Gaudin, Y. (2012). Molecular and cellular aspects of rhabdovirus entry. Viruses *4*, 117–139.

Andersen, O.S., and Koeppe, R.E., 2nd (2007). Bilayer thickness and membrane protein function: an energetic perspective. Annu. Rev. Biophys. Biomol. Struct. *36*, 107–130.

Barclay, A.N., and Van den Berg, T.K. (2014). The interaction between signal regulatory protein alpha (SIRPα) and CD47: structure, function, and therapeutic target. Annu. Rev. Immunol. *32*, 25–50.

Cabantous, S., Terwilliger, T.C., and Waldo, G.S. (2005). Protein tagging and detection with engineered self-assembling fragments of green fluorescent protein. Nat. Biotechnol. *23*, 102–107.

Campbell, L.A., Coke, L.M., Richie, C.T., Fortuno, L.V., Park, A.Y., and Harvey, B.K. (2019). Gesicle-mediated delivery of CRISPR/Cas9 ribonucleoprotein complex for inactivating the HIV provirus. Mol. Ther. *27*, 151–163.

Cavrois, M., De Noronha, C., and Greene, W.C. (2002). A sensitive and specific enzyme-based assay detecting HIV-1 virion fusion in primary T lymphocytes. Nat. Biotechnol. *20*, 1151–1154.

Chao, M.P., Weissman, I.L., and Majeti, R. (2012). The CD47-SIRPα pathway in cancer immune evasion and potential therapeutic implications. Curr. Opin. Immunol. *24*, 225–232.

Clarke, D.C., Betterton, M.D., and Liu, X. (2006). Systems theory of Smad signalling. Syst. Biol. (Stevenage) *153*, 412–424.

Clarke, D.C., and Liu, X. (2010). Measuring the absolute abundance of the Smad transcription factors using quantitative immunoblotting. Methods Mol. Biol. *647*, 357–376.

Cocucci, E., and Meldolesi, J. (2015). Ectosomes and exosomes: shedding the confusion between extracellular vesicles. Trends Cell Biol. *25*, 364–372.

Colletier, J.P., Chaize, B., Winterhalter, M., and Fournier, D. (2002). Protein encapsulation in liposomes: efficiency depends on interactions between protein and phospholipid bilayer. BMC Biotechnol. *2*, 9.

Cox, J., Hein, M.Y., Luber, C.A., Paron, I., Nagaraj, N., and Mann, M. (2014). Accurate proteome-wide label-free quantification by delayed normalization

and maximal peptide ratio extraction, termed MaxLFQ. Mol. Cell. Proteomics *13*, 2513–2526.

Dalton, K.P., and Rose, J.K. (2001). Vesicular stomatitis virus glycoprotein containing the entire green fluorescent protein on its cytoplasmic domain is incorporated efficiently into virus particles. Virology *279*, 414–421.

Doudna, J.A., and Charpentier, E. (2014). Genome editing. The new frontier of genome engineering with CRISPR-Cas9. Science *346*, 1258096.

Erickson, H.P. (2009). Size and shape of protein molecules at the nanometer level determined by sedimentation, gel filtration, and electron microscopy. Biol. Proced. Online *11*, 32–51.

Finkelshtein, D., Werman, A., Novick, D., Barak, S., and Rubinstein, M. (2013). LDL receptor and its family members serve as the cellular receptors for vesicular stomatitis virus. Proc. Natl. Acad. Sci. USA *110*, 7306–7311.

Fonseca, R., and Winter, P. (2012). Bounding volumes for proteins: a comparative study. J. Comput. Biol. *19*, 1203–1213.

Fu, A., Tang, R., Hardie, J., Farkas, M.E., and Rotello, V.M. (2014). Promises and pitfalls of intracellular delivery of proteins. Bioconjug. Chem. *25*, 1602–1608.

Hammond, S.M., Boettcher, S., Caudy, A.A., Kobayashi, R., and Hannon, G.J. (2001). Argonaute2, a link between genetic and biochemical analyses of RNAi. Science *293*, 1146–1150.

Haraszti, R.A., Didiot, M.C., Sapp, E., Leszyk, J., Shaffer, S.A., Rockwell, H.E., Gao, F., Narain, N.R., DiFiglia, M., Kiebish, M.A., et al. (2016). High-resolution proteomic and lipidomic analysis of exosomes and microvesicles from different cell sources. J. Extracell. Vesicles *5*, 32570.

Hirschberg, K., Miller, C.M., Ellenberg, J., Presley, J.F., Siggia, E.D., Phair, R.D., and Lippincott-Schwartz, J. (1998). Kinetic analysis of secretory protein traffic and characterization of Golgi to plasma membrane transport intermediates in living cells. J. Cell Biol. *143*, 1485–1503.

Hughes, C.S., Foehr, S., Garfield, D.A., Furlong, E.E., Steinmetz, L.M., and Krijgsveld, J. (2014). Ultrasensitive proteome analysis using paramagnetic bead technology. Mol Syst Biol *10*, 757.

Hung, M.E., and Leonard, J.N. (2016). A platform for actively loading cargo RNA to elucidate limiting steps in EV-mediated delivery. J. Extracell. Vesicles *5*, 31027.

Jeppesen, D.K., Fenix, A.M., Franklin, J.L., Higginbotham, J.N., Zhang, Q., Zimmerman, L.J., Liebler, D.C., Ping, J., Liu, Q., Evans, R., et al. (2019). Reassessment of exosome composition. Cell *177*, 428–445.e18.

Johnson, G.T., Autin, L., Goodsell, D.S., Sanner, M.F., and Olson, A.J. (2011). ePMV embeds molecular modeling into professional animation software environments. Structure *19*, 293–303.

Kamerkar, S., LeBleu, V.S., Sugimoto, H., Yang, S., Ruivo, C.F., Melo, S.A., Lee, J.J., and Kalluri, R. (2017). Exosomes facilitate therapeutic targeting of oncogenic KRAS in pancreatic cancer. Nature *546*, 498–503.

Köker, T., Fernandez, A., and Pinaud, F. (2018). Characterization of split fluorescent protein variants and quantitative analyses of their self-assembly process. Sci. Rep. *8*, 5344.

Komatsu, N., Aoki, K., Yamada, M., Yukinaga, H., Fujita, Y., Kamioka, Y., and Matsuda, M. (2011). Development of an optimized backbone of FRET biosensors for kinases and GTPases. Mol. Biol. Cell *22*, 4647–4656.

Kowal, J., Arras, G., Colombo, M., Jouve, M., Morath, J.P., Primdal-Bengtson, B., Dingli, F., Loew, D., Tkach, M., and Théry, C. (2016). Proteomic comparison defines novel markers to characterize heterogeneous populations of extracellular vesicle subtypes. Proc. Natl. Acad. Sci. USA *113*, E968–E977.

Le Blanc, I., Luyet, P.P., Pons, V., Ferguson, C., Emans, N., Petiot, A., Mayran, N., Demaurex, N., Fauré, J., Sadoul, R., et al. (2005). Endosome-to-cytosol transport of viral nucleocapsids. Nat. Cell Biol. *7*, 653–664.

Lefrancois, L., and Lyles, D.S. (1982). The interaction of antibody with the major surface glycoprotein of vesicular stomatitis virus I. Analysis of neutralizing epitopes with monoclonal antibodies. Virology *121*, 157–167.

Leung, A.K., Calabrese, J.M., and Sharp, P.A. (2006). Quantitative analysis of argonaute protein reveals microRNA-dependent localization to stress granules. Proc. Natl. Acad. Sci. USA *103*, 18125–18130.

Lodish, H.F., and Weiss, R.A. (1979). Selective isolation of mutants of vesicular stomatitis virus defective in production of the viral glycoprotein. J. Virol. *30*, 177–189.

Lomize, M.A., Lomize, A.L., Pogozheva, I.D., and Mosberg, H.I. (2006). OPM: orientations of proteins in membranes database. Bioinformatics *22*, 623–625.

Maeder, M.L., and Gersbach, C.A. (2016). Genome-editing technologies for gene and cell therapy. Mol. Ther. *24*, 430–446.

Mangeot, P.E., Cosset, F.L., Colas, P., and Mikaelian, I. (2004). A universal transgene silencing method based on RNA interference. Nucleic Acids Res. *32*, e102.

Mangeot, P.E., Dollet, S., Girard, M., Ciancia, C., Joly, S., Peschanski, M., and Lotteau, V. (2011). Protein transfer into human cells by VSV-G-induced nanovesicles. Mol. Ther. *19*, 1656–1666.

Mathieu, M., Martin-Jaular, L., Lavieu, G., and Théry, C. (2019). Specificities of secretion and uptake of exosomes and other extracellular vesicles for cell-to-cell communication. Nat. Cell Biol. *21*, 9–17.

Menck, K., Sönmezer, C., Worst, T.S., Schulz, M., Dihazi, G.H., Streit, F., Erdmann, G., Kling, S., Boutros, M., Binder, C., et al. (2017). Neutral sphingomyelinases control extracellular vesicles budding from the plasma membrane. J. Extracell. Vesicles *6*, 1378056.

Messenger, S.W., Woo, S.S., Sun, Z., and Martin, T.F.J. (2018). A Ca2+-stimulated exosome release pathway in cancer cells is regulated by Munc13-4. J. Cell Biol. *217*, 2877–2890.

Montagna, C., Petris, G., Casini, A., Maule, G., Franceschini, G.M., Zanella, I., Conti, L., Arnoldi, F., Burrone, O.R., Zentilin, L., et al. (2018). VSV-G-enveloped vesicles for traceless delivery of CRISPR-Cas9. Mol. Ther. Nucleic Acids *12*, 453–462.

Munis, A.M., Tijani, M., Hassall, M., Mattiuzzo, G., Collins, M.K., and Takeuchi, Y. (2018). Characterization of antibody interactions with the G protein of vesicular stomatitis virus Indiana strain and other Vesiculovirus G proteins. J. Virol. *92*, e00900–e00918.

Narendra, D.P., Jin, S.M., Tanaka, A., Suen, D.F., Gautier, C.A., Shen, J., Cookson, M.R., and Youle, R.J. (2010). PINK1 is selectively stabilized on impaired mitochondria to activate Parkin. PLoS Biol. *8*, e1000298.

Nelson, C.E., and Gersbach, C.A. (2016). Engineering delivery vehicles for genome editing. Annu. Rev. Chem. Biomol. Eng. *7*, 637–662.

Ran, F.A., Cong, L., Yan, W.X., Scott, D.A., Gootenberg, J.S., Kriz, A.J., Zetsche, B., Shalem, O., Wu, X., Makarova, K.S., et al. (2015). In vivo genome editing using Staphylococcus aureus Cas9. Nature *520*, 186–191.

Raposo, G., and Stoorvogel, W. (2013). Extracellular vesicles: exosomes, microvesicles, and friends. J. Cell Biol. *200*, 373–383.

Shalem, O., Sanjana, N.E., Hartenian, E., Shi, X., Scott, D.A., Mikkelson, T., Heckl, D., Ebert, B.L., Root, D.E., Doench, J.G., and Zhang, F. (2014). Genome-scale CRISPR-Cas9 knockout screening in human cells. Science *343*, 84–87.

Shalem, O., Sanjana, N.E., and Zhang, F. (2015). High-throughput functional genomics using CRISPR-Cas9. Nat. Rev. Genet. *16*, 299–311.

Sockolosky, J.T., Dougan, M., Ingram, J.R., Ho, C.C., Kauke, M.J., Almo, S.C., Ploegh, H.L., and Garcia, K.C. (2016). Durable antitumor responses to CD47 blockade require adaptive immune stimulation. Proc. Natl. Acad. Sci. USA *113*, E2646–E2654.

Thery, C., Amigorena, S., Raposo, G., and Clayton, A. (2006). Isolation and characterization of exosomes from cell culture supernatants and biological fluids. Curr. Protoc. Cell Biol. *30*, 3.22.1–3.22.29.

Tkach, M., and Théry, C. (2016). Communication by extracellular vesicles: where we are and where we need to go. Cell *164*, 1226–1232.

van Niel, G., D'Angelo, G., and Raposo, G. (2018). Shedding light on the cell biology of extracellular vesicles. Nat. Rev. Mol. Cell Biol. *19*, 213–228.

Votteler, J., Ogohara, C., Yi, S., Hsia, Y., Nattermann, U., Belnap, D.M., King, N.P., and Sundquist, W.I. (2016). Designed proteins induce the formation of nanocage-containing extracellular vesicles. Nature *540*, 292–295.

Wang, Y., Stary, J.M., Wilhelm, J.E., and Newmark, P.A. (2010). A functional genomic screen in planarians identifies novel regulators of germ cell development. Genes Dev *24*, 2081–2092.

Weissenhorn, W., Hinz, A., and Gaudin, Y. (2007). Virus membrane fusion. FEBS Lett *581*, 2150–2155.

Weissenhorn, W., Poudevigne, E., Effantin, G., and Bassereau, P. (2013). How to get out: ssRNA enveloped viruses and membrane fission. Curr. Opin. Virol. *3*, 159–167.

Yu, H., Crisman, L., Stowell, M.H.B., and Shen, J. (2019). Functional reconstitution of intracellular vesicle fusion using purified SNAREs and Sec1/Munc18 (SM) proteins. Methods Mol. Biol. *1860*, 237–249.

Yu, H., Rathore, S.S., Shen, C., Liu, Y., Ouyang, Y., Stowell, M.H., and Shen, J. (2015). Reconstituting intracellular vesicle fusion reactions: the essential role of macromolecular crowding. J. Am. Chem. Soc. *137*, 12873–12883.

Yu, H., Shen, C., Liu, Y., Menasche, B.L., Ouyang, Y., Stowell, M.H.B., and Shen, J. (2018). SNARE zippering requires activation by SNARE-like peptides in Sec1/Munc18 proteins. Proc. Natl. Acad. Sci. USA *115*, E8421–E8429.

Zelphati, O., Wang, Y., Kitada, S., Reed, J.C., Felgner, P.L., and Corbeil, J. (2001). Intracellular delivery of proteins with a new lipid-mediated delivery system. J. Biol. Chem. *276*, 35103–35110.

Zhang, C., Lee, S., Peng, Y., Bunker, E., Giaime, E., Shen, J., Zhou, Z., and Liu, X. (2014). PINK1 triggers autocatalytic activation of Parkin to specify cell fate decisions. Curr. Biol. *24*, 1854–1865.

Zhang, C., Lee, S., Peng, Y., Bunker, E., Shen, C., Giaime, E., Shen, J., Shen, J., Zhou, Z., and Liu, X. (2015). A chemical genetic approach to probe the function of PINK1 in regulating mitochondrial dynamics. Cell Res. *25*, 394–397.

Zhang, C., Liu, Z., Bunker, E., Ramirez, A., Lee, S., Peng, Y., Tan, A.C., Eckhardt, S.G., Chapnick, D.A., and Liu, X. (2017). Sorafenib targets the mitochondrial electron transport chain complexes and ATP synthase to activate the PINK1-Parkin pathway and modulate cellular drug response. J. Biol. Chem. *292*, 15105–15120.

Zomer, A., Maynard, C., Verweij, F.J., Kamermans, A., Schäfer, R., Beerling, E., Schiffelers, R.M., de Wit, E., Berenguer, J., Ellenbroek, S.I.J., et al. (2015). In vivo imaging reveals extracellular vesicle-mediated phenocopying of metastatic behavior. Cell *161*, 1046–1057.

Zuris, J.A., Thompson, D.B., Shu, Y., Guilinger, J.P., Bessen, J.L., Hu, J.H., Maeder, M.L., Joung, J.K., Chen, Z.Y., and Liu, D.R. (2015). Cationic lipid-mediated delivery of proteins enables efficient protein-based genome editing in vitro and in vivo. Nat. Biotechnol. *33*, 73–80.

Please cite this article in press as: Zhang et al., Programmable Extracellular Vesicles for Macromolecule Delivery and Genome Modifications, Developmental Cell (2020), https://doi.org/10.1016/j.devcel.2020.11.007

STAR★METHODS

KEY RESOURCES TABLE

REAGENT or RESOURCE	SOURCE	IDENTIFIER
Constructs		
pCMV-VSV-G-Myc	Neil King/University of Washington	N/A
pBbsr-VSV-G-sfGFP	This paper	N/A
pBbsr-VSV-G-GFP11	This paper	N/A
pBbsr-VSV-G-Myc-p6Gag-GFP11	This paper	N/A
pCMV-VSV-G-P127D-Myc	Neil King/University of Washington	N/A
pBbsr-VSV-G-P127D-Myc-p6Gag-GFP11	This paper	N/A
pBbsr-VSV-G-NJ-GFP11	This paper	N/A
pBbsr-VSV-G-Myc-Cre	This paper	N/A
pCMV4-BlaM-Vpr	Neil King/University of Washington	N/A
pBbsr-BlaM-Vpr-GFP1-10	This paper	N/A
pBbsr-Cre-GFP1-10	This paper	N/A
EGFP-hAgo2	Leung et. al., 2006	Addgene plasmid #21981
pBbsr-AGO2-GFP1-10	This paper	N/A
pBS-elav-1	Wang et al., 2010	Addgene plasmid #26130
pBbsr-Elav1-GFP1-10	This paper	N/A
pX602-AAV-TBG::NLS-SaCas9-NLS-HA-OLLAS-bGHpA;U6::BsaI-sgRNA	Ran et al., 2015	Addgene plasmid #61593
pBbsr-NLS-SaCas9-NLS-HA-GFP1-10	This paper	N/A
pBbsr-CD9-GFP11	This paper	N/A
pBbsr-CD81-GFP11	This paper	N/A
Lenti-CRISPR/Cas9-sgMunc13-4	This paper	N/A
pLKO-PINK1-shRNA	Zhang, et al, 2014	N/A
LentiCRISPR-EGFP sgRNA 1	Shalem et al., 2014	Addgene plasmid #51760
pEntry-bGH-U6-(SaCas9)-sgPINK1	This paper	N/A
pEntry-bGH-U6-(SaCas9)-sgEGFP	This paper	N/A
pEntry-bGH-U6-(SaCas9)-sgPCSK9	This paper	N/A
pEntry-bGH-U6-(SaCas9)-sgRosa26	This paper	N/A
pBbsr-CD47-Myc-GFP11	This paper	N/A
pBbsr-CD47nanobody-Myc-GFP11	This paper	N/A
Cell Lines		
293T	ATCC	Cat# CRL-1573
293ColorSwitch	This paper	N/A
HeLa	ATCC	Cat# CCL-2
HeLa-Venus-Parkin-RFP-Smac	Zhang, et al., 2014	N/A
HeLa-PINK1-EGFP	Zhang, et al., 2017	N/A
Antibodies		
Mouse anti-VSV-G (8G5F11)	Kerafast	Cat# EB0010; RRID: AB_2811223
Mouse anti-BlaM	Abcam	Cat# ab12251; RRID: AB_298974
Rabbit anti-GFP	Cell Signaling Technology	Cat# 2956; RRID: AB_1196615
Mouse anti-Myc tag	Cell Signaling Technology	9B11, Cat#2276
Rabbit anti-CD9	Cell Signaling Technology	Cat# 13174; RRID: AB_2798139
Rabbit anti-Flotillin	Cell Signaling Technology	Cat# 18634; RRID: AB_2773040
Rabbit anti-GM130	Cell Signaling Technology	Cat# 12480; RRID: AB_2797933
Mouse anti-Actinin4	Santa Cruz Biotechnology	Cat# sc-166524; RRID: AB_2257995

(*Continued on next page*)

Please cite this article in press as: Zhang et al., Programmable Extracellular Vesicles for Macromolecule Delivery and Genome Modifications, Developmental Cell (2020), https://doi.org/10.1016/j.devcel.2020.11.007

Continued

REAGENT or RESOURCE	SOURCE	IDENTIFIER
Mouse anti-TSG101	Santa Cruz Biotechnology	Cat# sc-7964; RRID: AB_671392
Rabbit anti-PINK1	Cell Signaling Technology	Cat# 6946; RRID: AB_11179069
Rabbit anti-Munc13-4	R&D Systems	Cat# MAB8966
Rabbit anti-Annexin V	Cell Signaling Technology	Cat# 8555; RRID: AB_10950499
Mouse anti-GAPDH	Santa Cruz Biotechnology	Cat# sc-47724; RRID: AB_627678
Mouse anti-β-actin	Santa Cruz Biotechnology	Cat# sc-47778 HRP; RRID: AB_2714189
Mouse anti-PCSK9	R&D systems	From the ELISA Kit
Anti-mouse IgG, HRP-linked Antibody	Cell Signaling Technology	Cat# 7076; RRID: AB_330924
Anti-Rabbit IgG, HRP-linked Antibody	Cell Signaling Technology	Cat# 7074; RRID: AB_2099233
Goat anti-Mouse IgG/M Gold 6nm	Electron Microscopy Sciences	Cat# 25123
Chemicals and Proteins		
PEI, Polyethylenimine	Sigma-Aldrich	CAS#9002-98-6
CCCP, Carbonyl cyanide m-chlorophenyl hydrazone	Sigma-Aldrich	CAS#555-60-2
GW4869	Cayman Chemical	Cat# 13127
Recombinant (*E. Coli*) rGFP protein	PROSPEC	Cat# pro-687-a
Protein-G Magnetic beads	Thermo Scientific	Cat# 88847
Protein-G Agarose beads	Thermo Scientific	Cat# 20397
Exosome Human CD9 Isolation kit	Life Technologies	Cat# 10614D
Aldehyde sulfate beads	Invitrogen	Aldehyde/Sulfate latex, 4% w/v 4μm
Primers and sgRNA		
5′-CACCGCCTGGAGGTGACAAAGAGCA-3′	Invitrogen	PINK1, Forward
5′-AAACTGCTCTTTGTCACCTCCAGGC-3′	Invitrogen	PINK1, Reverse
5′-CGCTGCTGCTGCGCTTCA-3′	Invitrogen	PINK1Ex1, Forward
5′-CTGCTCCATACTCCCCAGCC-3′	Invitrogen	PINK1Ex3, Reverse
5′-GTCTCCATAATCAGACACCT-3′	Invitrogen	PINK1Int2, Forward
5′-GGATGGTGAACTAACCAATC-3′	Invitrogen	PINK1Int3, Reverse
5′-GATGCCACTTTACTTCGGAGGA-3′	Invitrogen	mPCSK9, Forward
5′-AGGAGGATTGGAGTGGGGATTA-3′	Invitrogen	mPCSK9, Reverse
5′-CACCGAGGACCGCCCTGGGCCTGG-3′	Invitrogen	sgRosa26 Forward
5′-AAACCCAGGCCCAGGGCGGTCCTC-3′	Invitrogen	sgRosa26 Reverse
5′-CACCGCAGCCACGCAGAGCA-3′	Invitrogen	sgmPCSK9 Forward
5′-AAACTGCTCTTTGTCACCTCCAGGC-3′	Invitrogen	sgmPCSK9 Reverse
5′-CACCGCCTGGAGGTGACAAAGAGCA-3′	Invitrogen	sgPINK1 Forward
5′-AAACTGCTCTTTGTCACCTCAGGC-3′	Invitrogen	sgPINK1 Reverse
5′- CACCGCGAGACCTTCATCCTGTACG-3′	Invitrogen	sgMunc13-4 Forward
5′- AAACCGTACAGGATGAAGGTCTCGC-3′	Invitrogen	sgMunc13-4 Reverse
5′-CACCGTCGTGCTGCTTCATGTGGT-3′	Invitrogen	sgEGFP Forward
5′-AAACACCACATGAAGCAGCACGAC-3′	Invitrogen	sgEGFP Reverse
Commercial Kits		
GeneBLAzer In Vivo Detection Kit	Invitrogen	Lot# 1906803
Mouse Proprotein Convertase 9/PCSK9 Quantikine ELISA Kit	R&D systems	Cat# MPC900
Mouse LDL-Cholesterol Kit	Crystal Chem	Cat# 79980
ExoFlow-ONE EV Labeling Kit for Flow Cytometry	SBI System Biosciences	Cat# EXOFXXXA-1
TOPO TA-Cloning kit	Invitrogen	Lot# 1952884
Software		
ImageJ	NIH	N/A
GraphPad Prism 7	GraphPad Software	N/A
Blender	The Blender Foundation	N/A

(*Continued on next page*)

Please cite this article in press as: Zhang et al., Programmable Extracellular Vesicles for Macromolecule Delivery and Genome Modifications, Developmental Cell (2020), https://doi.org/10.1016/j.devcel.2020.11.007

Continued

REAGENT or RESOURCE	SOURCE	IDENTIFIER
BD FACSDiva	BD Biosciences	N/A
DAVID Bioinformatics Resources 6.8	NIAID/NIH	N/A
Deposited Data		
Proteomics data are reported in Table S2	This paper	N/A

RESOURCE AVAILABILITY

Lead Contact

Further information and requests for resources and reagents should be directed to and will be fulfilled by the Lead Contact, Xuedong Liu (Xuedong.Liu@colorado.edu).

Materials Availability

All unique generated in this study will be made available on request, but we may require a payment and/or a completed Materials Transfer Agreement if there is potential for commercial application.

Data and Code Availability

Label-free quantitative mass spectrometry data are provided in Table S2. All other relevant data are available from corresponding author (X.L.) upon request.

EXPERIMENTAL MODEL AND SUBJECT DETAILS

Animals

All mouse experiments were performed according to the protocol (No. 2667) approved by the IACUC office of the University of Colorado Boulder and the NIH guidelines. Female BALB/c mice (4 to 6 weeks old) from The Jackson Laboratory were used in Gectosome clearance and genome editing experiments.

Cell Culture

293T, 293ColorSwitch, RAW 264.7, and HeLa cell lines were obtained from the American Type Culture Collection (ATCC). All cell lines were cultured in Dulbecco's modified Eagle's medium (DMEM) supplemented with 10% FBS, 2 mM glutamine, 100 U/Ml penicillin, and 100 mg/mL streptomycin at 37°C with 5% CO2 incubation. 293T cells were used as the Gectosome producer cells. HeLa-Venus-Parkin-RFP-Smac and HeLa-PINK1-EGFP have been reported (Zhang et al., 2014, 2015, 2017). HeLa cells stably expressing Munc13-4 sgRNA were created using lentiviral particles from 293T cells transfected with lentiviral vector pLentiCRISPRv2-Munc13-4 sgRNA with three co-packaging plasmids (Zhang et al., 2014, 2015, 2017). 293ColorSwitch cell line was constructed by stable expression of the Cre reporter (Zomer et al., 2015). 293T and HeLa cell lines were validated by the University of Arizona Genetics Core Facility.

METHODS DETAILS

Gene Expression Constructs

A custom-built plasmid vector, called pBbsr-DEST, which contains the Gateway recombination sites, piggyback recombination sites, and IRES-blasticidin, was used for expressing genes in mammalian cells. pBbsr-DEST was constructed using the backbone of pPBbsr2 (a gift of Aoki and Matsuda) (Komatsu et al., 2011). For expression of the guide RNAs for SaCas9 or LwaCas13, platform-specific scaffolds were subcloned into an entry vector derived from pENTR221 (Invitrogen). Detailed maps of these parental vectors are available upon request. GFP11 and GFP1-10 fragments were first subcloned into pENTR and then recombined into pBbsr-DEST to yield pBbsr-GFP11 and pBbsr-GFP1-10 with stuffers. The cDNAs of VSV-G, VSV-G-NJ, CD9, CD81, CD47, CD47nb, HIV-p6Gag,GFP1-10 and GFP11 were obtained by gene synthesis (Twist Biosciences or BioBasic) and subcloned into pBbsr-GFP11. The cDNAs of BlaM-Vpr, Cre, AGO2, Elav and SaCas9 were subcloned into pBbsr-GFP1-10 from their source vectors. sgRNA expression vectors for PCSK9, Rosa26, PINK1, EGFP and Cre were constructed by inserting oligonucleotides synthesized into pEntry-U6-(SaCas9). siRNA PINK1 was synthesized by Dharmacon. sgMunc13-4 expression vector was constructed by inserting annealed oligos corresponding to the region of exon 6 in pLentiCRISPRv2-Puro.

Recombinant Protein Expression

Recombinant His-Flag-tagged Cre protein was expressed and purified in *E. coli* using pET28a vector and stored in a protein buffer (25 mM HEPES [pH 7.4], 150 mM KCl, 10% glycerol, and 1 mM DTT) (Yu et al., 2015). The recombinant Cre activity was determined as 1U/50ng according to the protocol from NEB (https://www.neb.com/protocols/2014/02/12/protocol-for-cre-recombinase-m0298).

Please cite this article in press as: Zhang et al., Programmable Extracellular Vesicles for Macromolecule Delivery and Genome Modifications, Developmental Cell (2020), https://doi.org/10.1016/j.devcel.2020.11.007

Production of Gectosomes

293T cells were seeded into 100 mm dishes and allowed to reach 70–80% confluence before transfection with polyethylenimine (PEI, 3 μL of PEI per μg DNA). Six hours after transfection, the medium was replaced with 10 mL of fresh DMEM. Supernatants were collected at 24 h or 48 h after transfection. For large scale production of Gectosomes for *in vivo* studies, Freestyle 293 Expression Medium (Thermo Fisher) was used instead of DMEM. The culture supernatants were harvested 48 h after transfection and then subject to centrifugation at 2,000 × *g* for 10 min. The resultant supernatant is referred to as the crude Gectosomes.

Flow Cytometric Analysis of Gectosomes

The size distribution of Gectosomes by flow cytometry using FACSAria Fusion Cell Sorter (BD). The crude Gectosomes were run on a FACSAria Fusion (Rate=20000 events/second) under FITC channel. The size reference beads from a kit (ExoFlow-ONE EV Labeling Kit for Flow Cytometry, SBI System Biosciences) were used as a standard size control. DMEM with 10% FBS, conditional control cultural supernatant, and the crude Gectosomes were diluted with ultrafiltered PBS (100KDa cutoff Amicon Ultra-15 Centrifugal Filter) to 1:100 and then submitted to flow cytometric analysis. 100,000 particles were collected for each sample. The gate was plotted according to the standard size reference beads where there were two groups colored with FITC. FITC-110 and FITC-500 are referred to as 110nm and 500nm size beads. The ratio of GFP-positive Gectosomes was analyzed with BD FACSDiva software.

Particle Size and Concentration Measurement by Nanoparticle Tracking Analysis (NTA)

NanoSight NS300 (NanoSight Ltd., UK) equipped with a high sensitivity sCMOS camera and NanoSight NTA 3.0 software was used to measure the size distribution and concentration of total particles of extracellular vesicles following the instructions of the manufacturer. The measurement parameters were as follows: temperature ranging from 21 to 23.6°C; viscosity between 0.9 and 0.965 cP, measurement time 60s, and 3 technical repeats (n=3). The measurement threshold was set at a similar level for all test samples. The data of total particles were obtained under the clear scatter measurement. We used 488 nm fluorescent filters to collect the data specific for fluorescent Gectosomes or exosomes. The results were shown as the mean sizes of particles plus standard deviations of three repeats.

Gectosome Release Assay

To confirm the release of Gectosomes from producer cells, we seeded 293T cells into a 6-well plate and transfected at 70–80% confluence with 1μg of pBbsr-VSV-G-GFP11 plus 2 μg pBbsr-BlaM-Vpr-GFP1-10 or Cre-GFP1-10 or AGO2-GFP1-10 or SaCas9-GFP1-10 using PEI. The media were replaced with 2 mL of fresh DMEM after 6 hr. Cell pellets and culture supernatants were collected 48 hr later. After removal of cell debris through centrifugation at 2,000 × *g* for 10 min, the released particles were collected through ultra-centrifugation with a 20% sucrose cushion for 90 min at 100,000 × *g* 4°C. The resultant pellets enriched with EVs were resuspended in 50uL of lysis buffer (50 mM Tris [pH 7.4], 150 mM NaCl, 1% Triton X-100, and a protease inhibitor cocktail (Roche)). The corresponding cell pellets were lysed for 30 min on ice in 100 μL of lysis buffer and clarified by centrifugation for 5 min at 12,000 rpm at 4°C to separate into the Triton-soluble and -insoluble cellular fractions. The EVs, Triton-soluble, and Triton-insoluble fractions were subjected to SDS-PAGE and immunoblotting analysis.

Immunoblotting Analysis

Protein concentration for cell extracts and vesicles was measured using the BCA assay (Thermo Fisher). Equivalent amounts of proteins were boiled in Laemmli sample buffer, resolved on 12% SDS-PAGE gels, and transferred to a 0.22μm nitrocellulose membrane. Membranes were blocked for 1 h in 5% non-fat dry milk (Nestle Carnation) or 5% bovine serum albumin depending on the primary antibody used. The filters were incubated with specific antibodies in Tris-buffered saline, 0.1% Tween 20 (TBST) overnight at 4°C. Antibodies used for Western blotting were as follows: anti-VSV-G (Mouse, 1:1000, Kerafast); anti-GFP (Rabbit, 1:1000, Cell Signaling Technology); anti-BlaM (Mouse, 1:1000, Abcam); anti-PINK1(Rabbit, 1:1000, Cell Signaling Technology); anti-GAPDH (1:2000, Santa Cruz Biotechnology); anti-CD9 (Rabbit, 1:1000, Cell Signaling Technology); anti-GM130 (Mouse, 1:1000, Cell Signaling Technology); anti-β-actin (Mouse, 1:2000, Santa Cruz Biotechnology); anti-Actinin4 (Mouse, 1:1000, Santa Cruz Biotechnology); anti-TSG101 (Mouse, 1:1000, Santa Cruz Biotechnology); anti-Annexin V (Mouse, 1:1000, Cell Signaling Technology); anti-Flotillin (Mouse, 1:1000, Cell Signaling Technology). Munc13-4 antibody (Rabbit, 1:1000, R&D systems). For chemiluminescence detection of proteins, HRP-conjugated anti-rabbit IgG (Cell Signaling Technology), and anti-mouse IgG (Cell Signaling Technology) secondary antibodies, and SuperSignal West Dura Substrate (Fisher Scientific) were used. ImageQuant LAS 4000 (GE HealthCare) was used to acquire images of the blots.

For quantitative immunoblotting experiments to determine the amount of VSV-G, Cre, and BlaM in Gectosomes, recombinant GFP protein (pro-687) was purchased from ProSpec, and recombinant β-lactamase (RP-431) was purchased from Alpha Diagnostic International. Recombinant Cre was prepared as described above. Serial dilutions of each recombinant protein were quantified by Coomassie blue staining along with a known amount of BSA to derive a standard curve for each protein.

BlaM and Cre Protein Cellular Uptake Assays

The β-lactamase (BlaM) cellular uptake assay was performed following the reported procedure (Votteler et al., 2016). Briefly, the indicated number of Gectosomes was incubated with HeLa or the mentioned cell lines seeded in 6-well plates for 16 hr or indicated time points. Cells were trypsinized, harvested, and spun at 1000 rpm for 5 min. Cell pellets were resuspended using 50 μL of CCF2-AM labeling solution prepared according to the manufacturer's instructions supplied with GeneBLAzer In Vivo Detection Kit (Thermo

Please cite this article in press as: Zhang et al., Programmable Extracellular Vesicles for Macromolecule Delivery and Genome Modifications, Developmental Cell (2020), https://doi.org/10.1016/j.devcel.2020.11.007

Fisher Scientific). Cells were labeled for 1 h at 25°C and then washed once with DMEM medium. The labeled cells in 500 μL fresh DMEM medium were analyzed by flow cytometry using BD FACSCelesta (BD Biosciences). 10,000 cells were collected for each sample. The fluorescence profiles in 488 nm and 405 nm channels were acquired and plotted using BD FACSDiva software. The mean percentages and standard deviations of three repeats were recorded.

For measuring Cre cellular uptake, 293ColorSwitch cells seeded on 6-well plates were used as target cells and incubated the indicated number of extracellular vesicles for 48 hr or indicated times. Following the incubation, cells were trypsinized, harvested, and scanned in 595 nm and 488 nm channels by flow cytometry using BD FACSCelesta (BD Biosciences). 10,000 cells were collected for each sample. The results were plotted with BD FACSDiva, and the mean percentages of green cells with standard deviations were recorded with three replicates (n=3).

Purification and Immobilization of the VSV-G Antibody

To purify the anti-VSV-G antibody, hybridoma cell line 8G5F11 (a gift of Douglas Lyles) was cultured in RPMI1640 for 3 days. The resultant supernatant was harvested by centrifugation at 2,000 × g for 5 min and subsequently filtered using a 0.2 μm filter to remove smaller cell debris. The cleared supernatant was incubated with Protein G-Agarose beads or Protein G-magnetic beads (Thermo Fisher) overnight. The antibody-bound beads were washed with PBS for 5 min three times, eluted with 100 μL 0.1M Glycine [pH 2.7], and neutralized with 1M Tris [pH9.5].

For conjugation of the VSV-G antibody to Protein G-Agarose beads or Protein G-magnetic beads, beads were incubated with the purified antibody overnight at 4°C and then washed with PBS to remove the unbound antibodies. Freshly made DMP solution (13 mg/mL Dimethylpimelimidate in Wash buffer, pH8-9) was added to beads at 1:1 ratio, and the mixture was rotated for 30 min at the room temperature. The conjugated beads were washed three times with the Wash buffer (0.2 M triethanolamine in PBS) at room temperature for 5 min per cycle. The conjugated beads were resuspended in PBS, and the labeling reaction was stopped by adding an equal volume of the quench buffer (50 mM ethanolamine in PBS). The beads were washed with 0.1 M glycine [pH 2.7] for 10 min twice and stored in PBS with 20% ethanol at 4°C until further use.

Isolation and Purification of Gectosomes

Isolation of EVs by Ultracentrifugation (UC)

The conditioned medium collected from cells growing on 100 mm plates was first cleared by low-speed centrifugation at 2,000×*g* for 10min (2K sample) to remove cell debris. The supernatant was centrifuged at 10,000×*g* at 4°C for 30 min (10k pellet), transferred to new tubes, and ultracentrifuged at 100,000×*g* in an SW41Ti (Beckman Coulter) at 4°C for 90 min (100k pellet).

Isolation of Gectosomes by Immunocapture

Cell conditioned medium was collected from confluent control or transfected 293T cells grown in Freestyle 293 Expression Medium on 100 mm culture dishes at 24 hr or 48 hr after transfection. The medium cleared by centrifugation at 10,000×*g* for 30 min at 4°C was incubated with magnetic beads or agarose beads containing the crosslinked 8G5F11 VSV-G antibody (8G5F11) at 4°C overnight. Beads bound with Gectosomes were washed with PBS for 5 min three times. Gectosomes were eluted with 0.1M Glycine [pH 2.7] and then neutralized with 1M Tris [pH9.5].

Purification of Gectosomes

0.5 mL of the cell-conditioned medium was processed as the above, except that supernatant from the 10,000 ×*g* spin was loaded onto IZON qEVoriginal column (IZON Science). Fractions (500 μL each) were collected using an Automatic Fraction Collector (IZON Science). Gectosomes were eluted in fractions 2 and 3, as determined by flow cytometry and immunoblotting analyses. Fraction 2 and 3 were combined and incubated with magnetic beads containing the crosslinked 8G5F11 VSV-G antibody. Gectosomes were eluted with 0.1M Glycine [pH3.7] and then neutralized with 1M Tris [pH9.5].

Fluorescence Microscopy

293T cells were seeded in a 96-well plate with glass bottom at 50% confluence and then transfected with plasmids encoding the split GFP system. 24 hours after transfection, cells were fixed with 2% paraformaldehyde in PBS containing DAPI (1.5 μg/ml DAPI). For imaging Gectosomes uptake, HeLa cells were incubated with Gectosomes for indicated times before fixation with 2% paraformaldehyde in PBS containing DAPI (1.5 μg/ml DAPI). Cells were stained with indicated primary and secondary antibodies before they were imaged with a laser scanning confocal microscope (Nikon A1R).

For the fluorescence switch imaging, 293ColorSwitch cells were seeded in a 96-well plate with glass bottom at 50% confluence before incubation with VSV-G/Cre Gectosomes. After 48 hours, cells were stained with Hoechst 33342 and imaged described above.

Negative Stain Transmission Electron Microscopy and Immunogold Labeling

TEM imaging and sample preparation were performed at the Electron Microscopy Services Core Facility of the University of Colorado Boulder.

Negative Stain TEM

Purified sfGFP and Cre Gectosomes through immunoaffinity procedure were applied to the negative stain. Briefly, 5 μL of the samples were firstly fixed in 4% paraformaldehyde for 1 hour, applied on a discharged, carbon-coated 400-mesh copper grid, and left it on for 3-5 minutes. The grid was washed in 1mM EDTA, and then 10 μL 0.75% uranyl formate is to be used for 1 minute for staining. The grid was subjected to TEM imaging.

Please cite this article in press as: Zhang et al., Programmable Extracellular Vesicles for Macromolecule Delivery and Genome Modifications, Developmental Cell (2020), https://doi.org/10.1016/j.devcel.2020.11.007

Immunogold Labeling TEM

Briefly, for immunogold labeling with anti-VSV-G, purified Gectosomes through immunoaffinity procedure were fixed for 1 h in 4% paraformaldehyde and then applied to a discharged, carbon-coated 400-mesh grid. The grids were then put onto a droplet of 1M Ammonium Chloride for 30 minutes. The samples on the grid were applied to immunogold labeling. The grids were rinsed for 5 min on large droplets of TBS-Tween (50mM TBS, 0.05% Tween 20, [pH 7.6]) for three times. The grids were incubated in block solution (1% BSA, 3% normal serum, 0.1% Fish Gelatin, 0.05% Sodium Azide in 0.05M TBS, [pH 7.6]) for 30 minutes. Then the grids were put into droplets of VSV-G antibody (1:50) (or mouse serum as control) diluted in block solution for 1 hour at room temperature. After rinsed the grids in large droplets of TBS-Tween for 5 min for three times, the grids were incubated in droplets of goat anti-mouse IgG/M 6nm (1:40) for 1 hour at room temperature. The samples on the grids were rinsed in droplets of TBS-Tween for 5 min three times. Lastly, a negative stain was performed as mentioned above. The images were recorded on a 120 kV Tecnai G2 Spirit transmission electron microscope at 52,000 × magnification.

Recombinant Cre Liposome Preparation

The preparation of recombinant Cre liposome was performed following the published procedure (Yu et al., 2018). Lipids used in this work were purchased from Avanti Polar Lipids. Briefly, 1-palmitoyl-2-oleoyl-sn-glycerol-3-phosphocholine (POPC), 1-palmitoyl-2-oleoyl-sn-glycerol-3-phosphoethanolamine (POPE), 1-palmitoyl-2-oleoyl-sn-glycerol-3-phosphoserine (POPS), and cholesterol were mixed in a molar ratio of 60:20:10:10. Cre proteoliposomes were prepared by the detergent dilution method. Complete detergent removal was achieved by overnight dialysis using Novagen dialysis tubes against the reconstitution buffer (25 mM HEPES [pH 7.4], 100 mM KCl, 10% glycerol, and 1 mM DTT) followed by liposome flotation on a Nycodenz gradient (Yu et al., 2019). The final concentration of Cre encapsulated in the liposome was determined by immunoblotting analysis using a serial dilution of a known amount of Cre as the standard.

Mass Spectrometry Analysis

Gectosomes immunocaptured on beads were boiled with 30 μL 1% SDS in 100 μM Tris-HCl [pH7.3] for 10 min and then submitted to mass spectrometry analysis. The samples were reduced and alkylated in 50 mM Tris-HCl, pH 8.5, containing 4% (w/v) SDS, 10 mM Tris(2-carboxyethylphosphine) (TCEP) and 40 mM chloroacetamide by boiling at 95°C for 10 min. Samples were then digested using the SP3 method (Hughes et al., 2014). Briefly, carboxylate-functionalized speedbeads (GE Life Sciences) were added to the extracts and then acetonitrile was added to 80% (v/v) to precipitate proteins onto the beads. The beads were washed twice with 80% (v/v) ethanol and twice with 100% acetonitrile. Proteins were digested on the beads in 20 μL 50 mM Tris-HCl [pH 8.5] and 0.5 μg Lys-C/Trypsin (Promega) incubating at 37°C for 18 hours with shaking at 1000 rpm. Digestion buffer was removed by adding acetonitrile to 95% (v/v) again, precipitating tryptic peptides onto the beads, followed by washing the beads once with acetonitrile. Peptides were removed from the beads in 50 μL 1% (v/v) trifluoroacetic acid and 3% (v/v) acetonitrile, then dried in a vacuum concentrator and stored at -20°C.

Samples were suspended in 15 μL 0.1% (v/v) trifluoroacetic acid and 3% (v/v) acetonitrile then 5 μL was directly injected onto a C18 1.7 μm, 130 Å, 75 μm X 250 mm M-class column (Waters) using a Thermo Scientific Ultimate 3000 RSLCnano UPLC. Peptides were eluted at 300 nL/minute using a gradient from 3% to 7% acetonitrile in 4 min, then 7% to 24% acetonitrile over 36 min into a Q-Exactive HF-X mass spectrometer (Thermo Scientific). Precursor mass spectra (MS1) were acquired at a resolution of 60,000 from 380 to 1580 m/z with an AGC target of $3x10^6$ and a maximum injection time of 45 ms. Precursor peptide ion isolation width for MS2 fragment scans was 1.4 m/z sequencing the top 12 most intense ions. All MS2 sequencing was performed using higher-energy collision dissociation (HCD) at 27% collision energy and scanning at a resolution of 15,000. An AGC target of 10^5 and 40 s maximum injection time was used for MS2 scans. Dynamic exclusion was set for 30 seconds with a mass tolerance of +/–10 ppm. MS data files were searched against the Uniprot human database downloaded 11/13/2019 with three additional sequences for VSV-G/GFP, β-lactamase and Cre using Maxquant version 1.6.3.4. Cysteine carbamidomethylation was set as a fixed modification, while methionine oxidation and protein N-terminal acetylation were set as variable modifications. All peptides and proteins were filtered at a 1% false discovery rate (FDR). Proteins identified by one or more specific peptides in either VB or VCB samples ($Q<0.001$) were included in Table S2 for the analysis.

RNA Interference by Gectosomes

Gectosomes loaded with *PINK1* shRNA were produced by transient transfection of 293T cells with *PINK1* shRNA plasmid (Zhang et al., 2014, 2017) along with expression plasmids VSV-G-GFP11 and AGO2-GFP1-10 or Elav-GFP1-10. The conditional culture supernatant containing Gectosomes (~$3x10^8$ particles/mL) was harvested, and 2 mL was incubated with target HeLa-Venus-Parkin-RFP-Smac cells (~$3x10^5$ cells/ well in a 6-well plate). After 24 hours, the culture supernatant was replaced with 2 mL of fresh media. After 3 days, Parkin localization on mitochondria in HeLa-Venus-Parkin-RFP-Smac cells in response to CCCP treatment was analyzed by method described below. Total RNAs were isolated using the Trizol method (Thermo Fisher Scientific). The levels of *PINK1* mRNA was measured by RT-qPCR analysis. The primers used in RT-qPCR were listed below: 5'-CACCGCCTGGAGGTGACAAAGAGCA-3' (*PINK1*, Forward), 5'-AAACTGCTCTTTGTCACCTCCAGGC-3' (*PINK1*, Reverse). *GAPDH* gene was used as the control. The *GAPDH* primers used were listed below: 5'- GAAGGTGAAGGTCGGAGT-3' (Forward) and 5'- GAAGATGGTGATGGGATTTC-3' (Reverse). Immunoblotting was used to probe the PINK1 protein level.

Please cite this article in press as: Zhang et al., Programmable Extracellular Vesicles for Macromolecule Delivery and Genome Modifications, Developmental Cell (2020), https://doi.org/10.1016/j.devcel.2020.11.007

Genome Editing with CRISPR/Cas9 Gectosomes

Gectosomes encapsulated with SaCas9-sgPINK1 (or mouse sgPCSK9) were produced by transient transfection of 293T cells with VSV-G-GFP11, SaCas9-GFP1-10 with guide RNA encoding plasmid sgPINK1 or mouse sgPCSK9. For *PINK1* editing in human cells, the conditioned culture supernatant containing the indicated Gectosomes (10^8 particles/mL) was harvested, and 2 mL of the supernatant was incubated with HeLa-Venus-Parkin-RFP-Smac and HeLa-PINK1-EGFP cells ($3x10^5$ cells/well in a 6-well plate). After 24 hours, the culture supernatant was replaced with 2 mL of fresh media. After treatment for five days, Parkin localization on mitochondria, protein levels, and mRNA levels of PINK1-EGFP in HeLa-Venus-Parkin-RFP-Smac and HeLa-PINK1-EGFP cells as described above. For *PCKS9* gene editing in mouse cells, MEF cells were incubated with Gectosomes loaded with SaCas9 and sgPCSK9.

To determine whether *PINK1* or *PCSK9* was edited in cells exposed to Gectosomes, the genomic DNA of the treated cells was extracted using the Blood and Tissue DNA Extraction kit (Qiagen) following the manufacturer's instructions. The primer sequences for *PINK1* gene target are: 5'- CGCTGCTGCTGCGCTTCA-3' (PINK1Ex1, Forward, for Exon PCR) and 5'- CTGCTCCATACTCCC CAGCC-3' (PINK1Ex3, Reverse, for Exon PCR), 5'- GTCTCCATAATCAGACACCT-3' (PINK1Int2, Forward, for intron PCR) and 5'-GGATGGTGAACTAACCAATC-3' (PINK1Int3, Reverse, for intro PCR), 5'-GATGCCACTTTACTTCGGAGGA-3' (mPCSK9, Forward) and 5'-AGGAGGATTGGAGTGGGGATTA-3'(mPCSK9, Reverse). PCR products were recovered and cloned using a TOPO TA Cloning Kit (Invitrogen). The colonies with insert fragments were sequenced and aligned with wild type genomic sequences, respectively.

Gectosome Clearance by Macrophage Cells

Gectosomes with CD47 or CD47nanobody were prepared from 293T cells seeded on 100 mm plates by transfecting 5 μg VSV-G-GFP11 plus 10 μg BlaM-Vpr-GFP1-10 with 5 μg CD47-GFP11 or 5 μg CD47nanobody-GFP11 plasmids. Gectosomes were harvested 48 hr post-transfection and cleaned up at 2,000 × *g* for 10min. Next, Gectosomes were incubated with RAW 264.7 cells for the indicated period. RAW 264.7 cells were subsequently removed to recover the supernatants, which were subsequently incubated with HeLa cells for 16 hr before the BlaM activity was measured by flow cytometry, as described above.

To directly measure the depletion of Gectosomes by macrophage, the particles were coupled to Aldehyde/Sulfate beads using a protocol (Thery et al., 2006) for flow cytometric analysis. Briefly, the supernatants recovered after incubation with RAW 264.7 cells were ultracentrifuged for 1.5 hr at 100,000×*g* at 4°C twice. The pellets were then resuspended in 200 μL PBS plus 10 μL of Aldehyde sulfate beads (Aldehyde/Sulfate latex, 4% w/v 4 μm, Invitrogen). 600 μL of PBS was then added to the mixtures and kept at 4°C on a tumbler overnight. Then 1M glycine (400 μL) was added to the mixture and incubated at room temperature for 1 hr. Beads were collected by brief centrifugation and washed three times with PBS plus 10% FBS before resuspended in 1 mL PBS with 10% FBS. The fluorescence intensity of Gectosomes immobilized on the beads was measured by flow cytometry.

Gectosome Clearance in Mice

To measure the Gectosome level in circulation *in vivo*, female BALB/c mice (4 to 6 weeks old) were injected intravenously with sfGFP Gectosomes produced with or without CD47 in 293T cells. The concentration of sfGFP positive Gectosomes in the supernatant was determined by NTA. Gectosomes were buffer-exchanged and concentrated to 10^{10} particles in 150 μL of PBS using ultrafiltration with the 100KDa cutoff Amicon Ultra-15 Centrifugal Filters). Concentrated Gectosomes were injected into BALB/c mouse (3 mice each group) through the tail vein. Three hours after injection, the injected mice were sacrificed to collect the EDTA-anticoagulated blood (150 μL) from mouse orbit. The blood samples were kept at room temperature for 1 hr prior to collecting the plasma by centrifugation at 3,000 rpm for 10 min at 4°C. Plasma (150 μL) was diluted to 5ml with PBS and ultracentrifuged 1.5 hr at 100,000×*g* at 4°C twice. The pellet was resuspended in PBS and mixed with aldehyde sulfate beads as described above. The rate of Gectosome depletion was measured by flow cytometry.

Genome Editing in Mice

Female BALB/c mice (4 to 6 weeks old) were ordered from The Jackson Laboratory. For the investigation of whether Gectosome delivery of the SaCas9-sgPCSK9 gene editing complex, the control and PCKS9 Gectosomes were prepared by transient transfection of 293T cells growing in Freestyle 293 Expression Medium. Gectosomes were concentrated approximately 100-fold by ultrafiltration using 100KDa cutoff Amicon Ultra-15 Centrifugal Filter Unit. Gectosomes were injected into 4-week-old female BALB/c mice via the tail vein. All dosages of Gectosomes were adjusted to 150 μL containing approximately 10^9 fluorescent Gectosomes in sterile phosphate-buffered saline. Mice received 10^9 particles/150 μL each tail vein injection for four times at 48 h of interval. For the measurement of the serum levels of PCSK9 and LDL-cholesterol, animals fasted overnight for 15 hr before blood collection by saphenous vein bleeds. Approximately 50μL blood was collected from each mouse every 10 days after injection. The serum was collected and stored at −20°C for subsequent analysis. Thirty days after injections all mice were sacrificed by carbon dioxide inhalation followed by cervical dislocation, and liver tissue samples were collected and stored at -80°C for subsequent DNA or protein extraction.

The level of PCSK9 protein in serum was determined by ELISA using a commercial ELISA kit (Mouse Proprotein Convertase 9/PCSK9 Quantikine ELISA Kit, MPC-900, R&D Systems) following the manufacturer's instructions. Serum LDL-cholesterol level was measured using a Mouse LDL-Cholesterol kit (Crystal Chem) per the manufacturer's instructions. Genomic DNA from mouse livers was isolated, and the *PCSK9* gene-editing analysis was carried out as described above.

Please cite this article in press as: Zhang et al., Programmable Extracellular Vesicles for Macromolecule Delivery and Genome Modifications, Developmental Cell (2020), https://doi.org/10.1016/j.devcel.2020.11.007

Mathematical Modeling of Gectosomes

Estimation of Protein Numbers in Gectosome

To determinate the abundance of VSV-G-GFP11 and Cre-GFP1-10 in Gectosome, we performed quantitative Western blot experiments and measured the expressed amount of VSV-G-GFP11, Cre-GFP1-10 proteins with recombinant protein stands. As shown in Figure S4E, there is about 7.47×10^{-7} ng VSV-G-GFP11, 9.73×10^{-8} ng Cre-GFP1-10 present per Gectosome when 293T cells were transfected with 1 μg VSV-G-GFP11, 2 μg Cre-GFP1-10, and 1 μg BlaM plasmids.

Therefore, in a Gectosome, we estimate that

$$\#VSV-G-GFP11=\frac{7.47\times10^{-7}\times10^{-9}}{8.0\times10^{4}}\times6.02\times10^{23}=5.62\times10^{3}\ molecules. \quad \text{(Equation 1)}$$

$$\#Cre-GFP1-10=\frac{9.73\times10^{-8}\times10^{-9}}{6.28\times10^{4}}\times6.02\times10^{23}=9.33\times10^{2}\ molecules. \quad \text{(Equation 2)}$$

3D Modeling for the Space-Filling of VSV-G-GFP11 and Cre-GFP1-10 Proteins in Gectosomes

The average measured diameter of single Cre Gectosome vesicles in this study is about 185 nm (Figure S2B). Here we assume that Gectosome vesicles are spherical. Considering that the bilayer thickness is about 2.5-3.5 nm and one side of the lipid head is about 1nm (Andersen and Koeppe, 2007), we estimate that the membrane thickness of a Gectosome is about 5 nm.

If we model VSV-G protein into the membrane in the Orientations of Proteins in Membranes (OPM) database (Lomize et al., 2006), the VSV-G protein attaches to the outer membrane surface of the vesicle. Cre-GFP1-10 will form a complex with VSV-G-GFP11 through an assumed irreversible complementation process; they are attached to the inner membrane of the Gectosome. We retrieved the protein structures of VSV-G monomer protein structure (PDB ID: 5I2S), sfGFP protein structure (PDB ID: 2B3P) and Cre recombinase monomer (PDB ID: 1NZB) in Blender with ePMV plugin (Johnson et al., 2011), which show the following dimensions of the bounding boxes.

(1) VSV-G,
x: 5.7 nm,
y: 4.9 nm,
z: 10.2 nm
(2) sfGFP,
x: 5.3 nm,
y: 4.8 nm,
z: 5.0 nm.
(3) Cre recombinase monomer,
x: 7.4 nm,
y: 6.5 nm,
z: 5.4 nm.

Figure S4E illustrates the relative size and orientation of different protein structures in a Gectosome.

The Occupancy of VSV-G Proteins at the Surface of Gectosomes

Based on the structure of VSV-G (PDB ID: 5I2S) monomer, the center of VSV-G was measured with a dimension of 5 nm (x-axis) and 4 nm (y-axis) and it is about 100 nm away from the center of Gectosome. We approximate this area as a circle with a diameter of 4.5 nm. Therefore, 5.62×10^{3} VSV-G proteins will occupy 71.1% of Gectosome surface based on the following calculation:

$$\frac{5.62\times10^{3}\times\pi\left(\frac{4.5}{2}\right)^{2}}{4\pi(100)^{2}}=71.1\% \quad \text{(Equation 3)}$$

The Occupancy of Cre-GFP Proteins Close to the Inner Membrane of a Gectosome

Based on the parameters shown in Figure S4E, we can estimate the volume of the intra-Gectosome sphere (V_i^t, excluding membrane) and the volume for the bounding hollow sphere that completely contains Cre and complemented GFP proteins ($V_{hs}^{Cre-GFP}$).

$$V_{hs}^{Cre-GFP}=\frac{4}{3}\pi(77.1+5+5.4)^{3}-\frac{4}{3}\pi(77.1)^{3}=8.86\times10^{5}\ (nm)^{3} \quad \text{(Equation 4)}$$

$$V_i^t=\frac{4}{3}\pi\left(\frac{185}{2}-5\right)^{3}=2.81\times10^{6}\ (nm)^{3} \quad \text{(Equation 5)}$$

Please cite this article in press as: Zhang et al., Programmable Extracellular Vesicles for Macromolecule Delivery and Genome Modifications, Developmental Cell (2020), https://doi.org/10.1016/j.devcel.2020.11.007

To estimate the space that is occupied by Cre and complemented GFP complex, we use protein bounding volume (Fonseca and Winter, 2012).

The bounding volume for one Cre monomer and one sfGFP protein is

$$V_b^{Cre-GFP} = 7.4 \times 6.5 \times 5.4 + 5.3 \times 4.8 \times 5 = 387\ (nm)^3 \quad \text{(Equation 6)}$$

The total bounding volume that 933 Cre-GFP molecules is

$$V_{tb}^{Cre-GFP} = 9.33 \times 10^2 \times 387 = 3.6 \times 10^5\ (nm)^3 \quad \text{(Equation 7)}$$

which is about 40.7% of the volume of bounding hollow sphere for Cre-GFP proteins ($V_{hs}^{Cre-GFP}$) and 12.9% of all the intra-Gectosome space volume (V_i^t).

3D Space-Filling of VSV-G-GFP11 and Cre-GFP1-10 Molecules in a Gectosome

We used an open-source 3D software Blender (https://www.blender.org) and the ePMV add-on to model the complemented VSV-G-GFP11 and Cre-GFP1-10 molecules in a Gectosome. The model is based on the space-filling model of the corresponding PDB protein structures at the nanometer scale. The protein structure of VSV-G, GFP11, and Cre-GFP1-10 monomers were represented with "Coarse Molecular Surface" by importing corresponding PDB structure file to ePMV in Blender. The unknown linker domains (e.g.: transmembrane domain) of the fused proteins were simplified as a cylinder, which links the VSV-G in the extra-Gectosome and the complemented sfGFP/Cre proteins. The outside view and the middle intersection view of the 3D model are illustrated in Figure 3F.

Estimation of the Partial Specific Volume for Proteins Identified from Mass Spectrometry Data

To quantify the relative abundance of the proteins found in the Gectosome, we used the label-free quantitation (LFQ) method based on the mass spectrometry data (Cox et al., 2014). The relative molar abundance of a protein was calculated by normalizing their LFQ values to the LFQ value for VSV-G protein. Based on the measured absolute abundance of VSV-G protein in Gectosome (5.62×10^3 molecules/Gectosome), we can convert the relative molar abundance to absolute quantification.

$$\#P_i = \frac{LFQ(P_i)}{LFQ(VSVG)} \times 5.62 \times 10^3 \quad \text{(Equation 8)}$$

Here we used the following empirical equation to calculate the partial specific volume of proteins based on their molecular weight (Erickson, 2009).

$$V(nm^3) = 1.212 \times 10^{-3}(nm^3 / Da) \times MW(Da) \quad \text{(Equation 9)}$$

To calculate the intra-Gectosome and extra-Gectosome protein volumes, we first identified the vesicle membrane proteins in the MS data using online software DAVID Bioinformatics Resources 6.8 (https://david.ncifcrf.gov/). The predicted partial specific volumes of the proteins in a Gectosome are listed in Table S2.

QUANTIFICATION AND STATISTICAL ANALYSIS

Image Analysis

The size of Gectosomes from TEM image was measured by using SerialEM software on transmission electron microscopy. The quantitative analysis of the colocalization of complemented split GFP (VSV-G-GFP11/Cre-GFP1-10) and EEA1(n=37) or Lamp1(n=47) in HeLa cells were performed using the Jacop Plugin of ImageJ and the data are expressed as a Pearson's coefficient (r).

Statistical Analysis

Statistical analyses of data were performed with GraphPad Prism 7. Data are represented as mean ± standard deviation or mean ± SEM or average ± standard error as indicated. For comparisons between two groups, statistical significance was determined using an unpaired student's t-test. The two-way ANOVA was used to compare the effects of different groups of treatments on PCSK9, LDL-cholesterol, and body weight of animals. Parkin localization on mitochondria was assessed with the MetaXpress application module called Transfluor Cell Scoring Application Module (Molecular Devices). Flow cytometric analysis was typically performed in three technical replicates (n=3) and the number of biological replicates is indicated for specific experiment in figure legends. Specific sample sizes, including the number of particles, cells, mice in each experiment, and *p-value*s are indicated in figures and figure legends.